MICROWAVE OPTOELECTRONICS

MATÁV · antenna hungária · SIEMENS Siemens Telefongyár Kft · ERICSSON · NOKIA · MOTOROLA · hif Communication Authority, Hungary · WESTEL RÁDIÓTELEFON KFT · PANNON GSM · TKI · FOUNDATION FOR THE "DEVELOPMENT OF CONSTRUCTION" · BHG BUDAPEST

EDITORIAL

Microwaves and photonics are among the fastest growing disciplines in engineering and physics. This special issue addresses the interface of these emerging technologies. There is an increasing interest in the interaction of microwaves and lightwaves in semiconductor materials, devices, circuits and systems. This interest has been generated partially by the availability of new, high speed, electrooptic devices (diode lasers, modulators, photo-diodes, switches, etc.) and partially by the development of more sophisticated microwave and millimeter-wave circuits and systems.

Microwave optoelectronics offers new potentials for the improvements in both microwave and optical systems. Optical control of microwave circuits, optical feed of microwave antennas, optical transmission of microwave signals are typical examples for it.

New applications are offered by the new aspects of the interaction processes. The interaction processes are divided into two parts: into the optical to microwave and the microwave to optical processes. However, in many cases both types of interaction processes are applied like in the optical transmission of microwave signals and in the combined optical-microwave signal processing. The application of optical solutions is advantageous because the optical circuits can be integrated into the microwave circuits without interfering with them, they have low losses and small dimensions, short reaction time, and wide transmission band.

In this special issue specific topics are presented by some well known experts of the field. These selected topics naturally don't cover the very broad area of microwave optoelectronics, however, the papers give us a flavor of the problems what can be solved utilizing the procedures of microwave optoelectronics. The present special issue provides new and interesting results.

The optical transmission can advantegously be used in a cellular or pico-cellular mobile communications system. The radio frequency of mobile systems is gradually increasing and therefore the optical link has to carry high microwave or millimeter-wave frequencies. That requires improvements in the laser diode transmitter, in the fiber — what is usually the transmission medium — and in the optical receiver.

The *first paper* deals with the system aspects of optical millimeter-wave generation techniques for broadband radio access networks. The system performance is analyzed considering the major sources of impairments.

The *second paper* present a novel technique for the generation of optical pulse trains with millimeter-wave repetition frequency. This method uses the nonlinear properties of a Mach-Zehnder intensity modulator to quadruple the pulse repetition frequency in an actively mode-locke erbium-doped fiber ring laser.

In the *third paper* a special kind of photodetector is discussed which is used for high power nonlinear heterodyne mixing of two optical signals, their difference fequency is in the millimeter-wave range. For that purpose a travelling wave structure is applied including a periodic array of nonlinear Schottky diodes.

In the *next paper* design problems of an optically controlled semiconductor coplanar-strip waveguide attenuator/modulator are studied based on a quasi static field distribution and a simple model of optically induced attenuation.

Application of analog fiber-optic links is the topic of a *further paper*. This paper presents an overview of analog optical links based on their three application areas: transmit, distribution and receive links.

A possible new reception method utilizing optical-microwave mixing processes is introduced in the *next paper*. Two types of the mixing processes are investigated both theoretically and experimentally.

Two further papers discuss the noise problems of broadband optical receivers and the transmission impairments of dispersive fibers.

In a *short paper* a continuous-time programmable-gain logarithmic photoreceptor cell is presented for parallel VLSI image processing.

We hope that with this special issue the readers will get new impression and knowledge about the fast growing area of microwave optoelectronics.

T. BERCELI
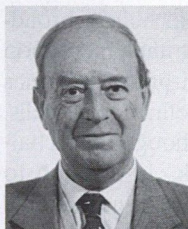
Tibor Berceli graduated in electrical engineering at the Technical University of Budapest, Hungary in 1951. In 1955 he received the Candidate of Technical Science, and in 1965 the Doctor of Technical Science degrees from the Hungarian Academy of Sciences. Dr. Berceli joined the TKI, Research Institute for Telecommunications, Budapest in 1951. Since that time he investigated surface wave transmission lines, dielectric waveguides, travelling wave tube amplifiers, reflex klystron oscillators, several kinds of microwave semiconductor oscillators and amplifiers, parametric circuits, up- and down-converters, injection locked oscillators, etc. His present field of interest is the optical-microwave interaction. Since 1962 he head a part time job at the TUB. Now he is Professor of Electrical Engineering there. He has courses on optical-microwave techniques, active nonlinear microwave circuits, and radio communication systems. Prof. Berceli is Fellow of IEEE. He was Chairman of the Organizing Committee for the URSI International Symposium on Electromagnetic Wave Theory in 1986, and Conference Chairman of the 20th European Microwave Conferencei in 1990. He is the author of 106 papers and 6 books published in English. He presented 76 papers at international conferences. He was visiting professor at Polytechnic Institute of Brooklyn in 1964, University College London in 1986, Drexel University (Philadelphia) in 1988-89, Technical University of Hamburg-Harburg in 1991, Osaka University in 1992, and Technical University of Grenoble in 1994.

OPTICAL MILLIMETER-WAVE GENERATION TECHNIQUES FOR BROADBAND RADIO ACCESS NETWORKS

R. A. GRIFFIN, P. M. LANE and J. J. O'REILLY

TELECOMMUNICATIONS GROUP, DEPARTMENT OF ELECTRONIC AND ELECTRICAL ENGINEERING
UNIVERSITY COLLEGE LONDON
TORRINGTON PLACE, LONDON WC1 E 7JE, UK

We review optical millimeter-wave generation for application in the photonic transport of data in broadband access networks. Performance is analyzed considering major sources of impairments.

1. INTRODUCTION

The provision of a radio link for the final drop in broadband customer access networks offers potential for rapid deployment, low cost-per-customer, and minimal maintenance. The millimeter-wave band is currently uncluttered and will support large bandwidths; utilization of frequency bands around 30 GHz and 60 GHz is currently under consideration. The system which we consider here involves the use of photonic technology for the transport of mm-wave signals from a central base station to multiple remote antenna units, merging photonic, microwave and digital radio technology [1]. This approach is currently being pursued by the FRANS project, a collaborative research project within the European Commission ACTS program.

The use of photonic technology for centralized signal distribution eases the requirements of the antenna unit functionality and provides transparent mapping of signals from the base station to the mm-wave radio spectrum. Each antenna unit provides only photodetection, amplification and filtering of the downlink signal before broadcast; MMIC technology will allow low cost implementation of these functions. Integrated, high gain patch antennas can provide efficient coverage of well-defined pico-cells. Operation in the mm-wave domain does though pose challenges for the design of the photonic link. In addition to generation of mm-wave optical signals, the requirements for transparency to data format and impairments inherent to the fibre link present some difficulty.

In this paper we consider the generation of optical mm-wave carrier signals, together with the imposition of data and delivery over fibre. In Section 2 we provide a brief overview of potential optical mm-wave sources. In Section 3 we consider system impairments. Using these considerations, in Section 4 we focus on a mm-wave generation technique which appears viable, and provide a detailed analysis of the implementation and performance of this approach.

2. SURVEY OF ALTERNATIVE GENERATION TECHNIQUES

Over recent years there has been a proliferation of techniques developed for the generation of optical millimeter-wave signals. Fibre-supported radio has been one of the main influences driving interest in this area. In this section alternative techniques are briefly described and broadly categorized. Although some approaches may be performed with various types of lasers, we assume the use of semiconductor lasers, which appear to offer the most potential for practical, low cost mm-wave system implementation.

2.1. Direct Laser Amplitude Modulation

Broadband Devices

A key feature of semiconductor lasers is their ability to support direct intensity modulation at high frequencies. The development of high bit rate optical links has driven the development of lasers with bandwidths spanning the microwave spectrum. Current state-of-the art is a bandwidth of 30 GHz [2]. Although further increase in bandwidth is likely, packaged devices with bandwidths of 60 GHz and beyond — seen as requirements for mm-wave radio access networks — are unlikely to be available in the near future.

Resonant Enhancement

An alternative approach to ultra-fast broadband lasers is to modify the frequency response of a lower-bandwidth device so as to enhance the modulation response at a particular desired frequency. This approach has been demonstrated using an external cavity to produce a resonant response at mm-wave frequencies. A more practical implementation has also been demonstrated using an extended-cavity DFB laser [3].

2.2. Mode-Locking

Mode-locking is a special case of resonant modulation as described above. The laser is again driven with a frequency matched to the optical round-trip time of the laser cavity, which may be an external or extended cavity. In this case, however, a wavelength-selective element is included in the laser cavity to limit the number of longitudinal laser modes. Resonant modulation fixes the relative phase between adjacent modes, producing an output train of short pulses at a repetition frequency equal to the modulation frequency. Depending on the number of modes, the output pulses may be much shorter than

the repetition rate, and hence produce substantial power at harmonics of the modulation frequency when incident on a photodetector [4].

2.3. Gain-Switching

Gain-switching is an alternative means of producing short pulses with high harmonic content. This approach relies on the nonlinear interaction between carrier and photon populations when the laser is driven with a large modulation signal at high frequency [5]. Gain-switching produces a pulse train similar to that achieved by mode-locking, but the time-bandwidth product for the gain-switched pulses may be substantially higher than for mode-locked pulses.

2.4. Frequency Modulation

The large FM index displayed by certain laser devices provides the possibility of opto-electronic frequency multiplication. By modulating at a frequency f_1, optical sidebands are produced separated by nf_1 around the optical carrier frequency. To provide intensity modulation at the photodetector, there are two alternative approaches:
- an optical filtering element, e.g. a Fabry Perot, is used to select the desired sidebands;
- fibre dispersion is utilized to perform FM-IM conversion [6]. This approach, however, is then strongly sensitive to fibre link length.

2.5. External Modulation

External modulation provides an obvious alternative to direct laser modulation and can circumvent fundamental laser bandwidth restrictions. Electro-optic devices based on $LiNbO_3$ are now reasonably mature, and there have been rapid developments in III-V devices. Small-signal bandwidths covering the mm-wave spectrum have been demonstrated, and techniques which utilize nonlinearities to perform frequency multiplication make use of commercially-available devices realistic.

Linear Modulation

The basic operation of Mach–Zehnder modulators relies on a linear electro-optic effect. An applied voltage changes the refractive index of the EO material, producing a phase shift for the optical signal propagating in the material. An integrated optic Mach–Zehnder structure transforms the induced optical phase shift to a change in intensity, with the device exhibiting a raised-cosine intensity-voltage characteristic.

With a dc bias of $V_{\pi/2}$, a linear intensity-voltage response is achieved for small modulations. The intrinsic bandwidth of the electro-optic effect in $LiNbO_3$ is very high; the practical difficulty for the construction of mm-wave modulators is to achieve velocity matching between propagating optical and electrical waves over the electrode interaction length. Modulation frequencies up to 100 GHz have been demonstrated, but the problem of velocity matching results in optical insertion loss, drive power requirements and unit cost increasing concomitantly with device bandwidth.

Non-Linear Modulation

Although the raised cosine response may be a disadvantage in limiting the usable linear modulation depth, the response can be utilized to achieve harmonic conversion. By biasing the MZM at V_π, the point of minimum transmission, a frequency doubling effect can be achieved. This approach provides the possibility of 60 GHz operation with commercially available devices [7]. The inherent nonlinearity of the MZM may also be utilized to provide a mixing function, allowing the tasks of data modulation and mm-wave generation to be achieved with a single device [8].

Electro-Absorption Modulation

Although $LiNbO_3$ technology is reasonably mature, there are still problems of device stability which are undesirable for system implementation. More recently, devices based on III-V technology have been developed as an alternative. Although MZM structures based on phase modulation can also be produced, III-V materials offer the possibility of electro-absorption operation utilizing the Franz–Keldysh effect in bulk material or the Quantum-Confined Stark effect in multiple quantum well structures. These devices exhibit greater nonlinearity and provide the possibility of more efficient harmonic generation [9].

2.6. Two-Laser Heterodyne Approaches

A class of techniques which provides great scope for signal generation is based on heterodyning two CW lasers. Consider the mixing of two optical fields $E_1 e^{i2\pi f_0 t}$ and $E_2 e^{i2\pi(f_0 + \Delta f)t}$ on a square-law photodetector. The frequency of the generated beat signal, Δf, is equal to the difference in optical frequency, and in principle can be varied throughout the mm-wave band.

Optical Frequency-Locked Loop

DFB semiconductor lasers are single-mode and widely tunable, and it is reasonably straightforward to control the optical difference frequency.* A problem with this approach, however, is laser phase noise. Although the phase noise of the optical carrier is relatively small, when mixed down to a microwave frequency by heterodyning, the generated signal shows poor purity. Techniques to reduce laser phase noise generally reduce either the robustness or the tunability compared to a monolithic laser.

Optical Phase-Locked Loop

One technique which has been used to improve signal purity is the optical phase-locked loop (OPLL). This approach does not reduce the laser phase noise, but employs a portion of the detected beat signal which is mixed with a local oscillator, filtered and fed back to a slave laser to track the phase fluctuations of the master laser. Since the phase fluctuations are correlated, the detected beat signal exhibits good spectral purity [10]. The fundamental problem with implementation is that loop gain-bandwidth, and hence phase noise reduction, is limited by the practically-achievable loop delay.

Optical Feed-Forward Modulation

This technique achieves the same effect as the OPLL, but feeds the generated error signal forward to a MZM in one laser path. The feed-forward structure overcomes the problem of loop delay minimization, but has strict requirements on delay matching [11].

Optical Injection Locking

This approach to phase noise reduction is more completely optical, but is also more complex. Firstly, multiple side-bands are induced in a seed laser, either by direct or external modulation. This signal is then fed to two frequency-controlled lasers whose free-running optical frequencies are matched to sidebands separated by the desired frequency. With sufficient seed power, the phase noise of the two slave lasers then becomes correlated [12].

2.7. Two-Mode Laser

Based on the two-laser heterodyning technique, signal generation can also be achieved by beating together two independent laser modes generated in a single laser cavity. Dual mode operation with appropriate frequency separation has been demonstrated in DFB semiconductor lasers employing either strong unshifted gratings, chirped gratings, or two-section construction. Although this approach seems to offer potential for a compact and robust source, results to date suggest the phase noise of simultaneously lasing modes is uncorrelated, and the beat signal displays poor purity. Improvement has been demonstrated using electrical modulation at a sub-harmonic to achieve injection locking, but at the expense of more complex optical spectra [13].

2.8. Optical Non-Linearity

Optical nonlinear effects have also been considered for optical microwave generation, the high power densities in single mode fibre and long interaction lengths making nonlinear effects significant.

Stimulated Brillouin Scattering (SBS) is an obvious candidate: acousto-optic interaction produces backscattered light with a frequency shift of some 10 GHz, suggesting the possibility of an all-optical passive generation technique. Apart from the practical problem of achieving efficient cascaded SBS, however, the main obstacle to this approach is the lack of tuning. Although the SBS frequency shift demonstrates some variation with wavelength, fibre composition and temperature, limited tuning severely restricts the utility of this approach.

An alternative nonlinear effect which can be very efficient in fibre is Four-Wave Mixing (FWM). Starting with an input two-tone optical spectrum, FWM generates successively higher sidebands of the optical spectrum for high power density × fibre length [14]. Although this suggests an appealing way to achieve all-optical frequency multiplication of an input signal, the requirement of providing initial modulation and the need for high power optical amplifiers suggests this approach will have limited application..

3. IMPAIRMENTS

Much of the published work on optical mm-wave generation has been device-oriented, and focused on the generation of a mm-wave carrier. For application to a broadband access network, however, it is obviously necessary to impose data on the optical signal. Further, it is essential to provide a high signal-to-noise ratio at the output of the fibre span to avoid degradation of overall system performance. These system-oriented considerations have been widely ignored. In this section we consider the main impairments which affect the performance of optical mm-wave delivery. While certain impairments may affect any generation technique, our aim is to identify generation techniques which appear to be most appropriate for system applications, and provide realistic estimate of performance.

3.1. Dispersion

The potential impairment due to fibre chromatic dispersion is an obvious consideration when considering transport of optical mm-wave signals. Although a range of techniques have been developed in recent years to mitigate dispersion penalties, these approaches have addressed transport of baseband digital data in the trunk network, and are not necessarily appropriate for access networks employing mm-wave carriers.

Firstly, consider the optical signal produced by external modulation of a CW single-mode laser with an ideal Mach−Zehnder modulator biased for linear intensity. The optical power spectrum can be written

$$S(f) = \frac{P_0}{2} \left\{ \sum_{n=-\infty}^{\infty} J_{2n}^2(m)\delta(f - f_0 - 2nf_{mm}) + \right.$$

$$\left. \sum_{n=-\infty}^{\infty} J_{2n+1}^2(m)\delta[f - f_0 - (2n+1)f_{mm}] \right\} \quad (1)$$

where f_0 is the mean optical frequency and P_0 is the total optical power, J_n represents the Bessel function of the first kind of order n, and m is the modulation index. The effect of fibre dispersion can be evaluated by expanding the propagation constant in a Taylor series around the centre frequency. Propagation through dispersive fibre results in repetitive length-dependent nulls in the detected signal power. The first null occurs at a fibre length L meters, given by

$$L = \frac{c}{2Df_{mm}^2\lambda_0^2} \quad (2)$$

where D [ps/(nm.km)] is the dispersion parameter, f_{mm} (GHz) is the mm-wave carrier frequency, λ_0 (μm) is the mean source wavelength, and c (m/s) is the vacuum velocity of light [3]. Millimeter-wave operation at 1550 nm and dispersion of 17 ps/nm.km — typical for standard single-mode fibre at 1550 nm — is therefore restricted to fibre lengths of less than 3 km at 30 GHz and less than 800 m at 60 GHz if large power penalties are to be avoided. Hence it is necessary to consider alternatives which may mitigate this problem.

1300 nm Operation

The zero dispersion wavelength (ZDW) of standard fibre falls in a window centered around 1310 nm, so it would seem a reasonable alternative to specify operation at this wavelength. An important consideration, however, is signal distribution to multiple sites. It is clear that optical amplification is necessary to allow each base station to serve multiple antenna units, allowing system cost to be shared among many customers. The most attractive optical amplifier technology is though Erbium-doped fibre amplifiers (EDFAs), operating in the 1550 nm window. Alternative rare-earth doped glasses are being developed for 1300 nm amplification, but it is doubtful if performance will match that of EDFAs. Semiconductor amplifiers are also developing, but an issue here is the possible degradation due to intermodulation distortion. Further, the significance of fibre loss should also be considered; values of .35 dB/km and .25 dB/km are typical for 1300 and 1550 nm respectively. For a fibre span of 30 km, the difference amounts to 3 dB. Thus 1300 nm operation could support only half the number of customers, even assuming optical amplifiers with the same characteristics as EDFAs are available.

1550 nm Operation

• *Dispersion Compensation*

This area has seen rapid development recently, and either chirped Bragg gratings or dispersion compensating fibre could be applied. Given the point-to-multipoint nature of our system, however, we would require either

• a tailored compensating device at each antenna unit matched to the particular fibre span length;

• a centralized compensator, with the span lengths to all antenna units tightly matched.

These requirements seem inconsistent with the need for a low cost, flexible access network, which may be required to utilize dark fibre.

• *Dispersion Assisted Transport*

It was outlined in Section 2.4 that fibre dispersion may be utilized to perform FM-IM conversion. This has been demonstrated [6], but the difficulty is the need for control of fibre length. It has also been noted that the periodic fading provides the possibility of operation over long lengths of fibre provided suitable control of the length is achieved. Again, this approach seems impractical, and limits the available signal bandwidth.

• *Dispersion Tolerant Transport*

Eq. (2) highlights the importance of dispersion for optical mm-wave transport. The maximum length of fibre in (2) is calculated assuming a large-carrier double-sideband optical spectrum resulting from external modulation. A sub-class of the optical mm-wave generation techniques, however, have a simpler spectrum consisting of only two discrete tones, separated by the mm-wave frequency:

$$S(f) = \frac{P_0}{2} \left[\delta \left(f - f_0 + \frac{f_{mm}}{2} \right) + \right.$$

$$\left. \delta \left(f - f_0 - \frac{f_{mm}}{2} \right) \right] \qquad (3)$$

Mixing of two phase-correlated tones at a square-law photodetector provides a spectrally pure mm-wave carrier signal at frequency f_{mm}. Fibre dispersion only affects the phase of the detected mm-wave signal and does not induce length-dependent fading of the signal power. As a result, standard fibre can be utilized at 1550 nm. In this case, there is no dispersion- induced power penalty, and the approach will operate over arbitrary lengths of standard fibre. Dispersion tolerance provides a strong criterion for selection of potential techniques, and hereafter we focus on techniques which provide the desired two-tone optical spectrum.

The sub-class of techniques which provide the desired spectra include the two-laser heterodyne techniques and two-mode lasers. Some of the other techniques, mode-locking, FM-modulation, and nonlinear multiplication, can be configured to produce two tones with the addition of a Fabry-Perot optical filter, but the added complexity and inefficiency resulting from discarding the majority of the signal do not make these approaches as attractive as those that are inherently two-tone. Harmonic conversion using an external modulator also falls into the two-tone subclass. Whereas linear external modulation results in a dispersion-sensitive double-sideband large-carrier spectrum, nonlinear modulation can be utilized to provide a two-tone spectrum. This point will be developed more fully in Section 4.

3.2. Phase Noise

Phase noise of the generated mm-wave carrier can degrade system performance, and hence it is essential that generation techniques address this requirement. In particular, this consideration must be applied to two-mode and two-laser generation techniques. Optical frequency-locked-loops are ruled out unless very narrow linewidth lasers are employed, since optical phase noise is converted directly to the mm-wave carrier. Optical PLLs provide considerable improvement, but measurement of phase noise for the best device reported to date [10] shows unacceptable levels of phase noise for broadband applications. External modulation approaches, however, achieve excellent phase noise performance due to the fact that the phase noise of optical tones which beat together is perfectly correlated.

3.3. Phase-Induced Intensity Noise

Phase-induced intensity noise (PIIN) arises from the interaction between laser phase noise and chromatic dispersion. As a mm-wave modulated optical signal propagates over fibre, chromatic dispersion introduces a time delay between discrete optical tones. The resulting reduced correlation has little impact on the magnitude of the detected beat signal, but is manifested in the conversion of optical phase noise to wideband intensity noise, with concomitant reduction in carrier-to-noise ratio (CNR) of the mm-wave signal. The significance of this term has not been widely appreciated for these systems.

3.4. Optical Amplifier Noise

A single optical amplifier may provide signal for up to

20 antenna units, sharing the cost of a central base station among many customers. Current technology makes the choice of Erbium-doped fibre amplifiers compelling. Optical amplifiers also generate amplified spontaneous emission (ASE) noise, however, which may impact system performance [16]. From the ASE noise power spectrum of the amplifier, the electrical noise power resulting from the signal-spontaneous beat noise and spontaneous-spontaneous beat noise at the photodiode can be calculated using the following equations:

$$P_{s-sp} = 2I_{ASE}I_s \frac{B_e}{B_0} \qquad (4)$$

$$P_{sp-sp} = I_{ASE}^2 \frac{B_e}{B_0} \qquad (5)$$

where B_e is the electrical bandwidth of the receiver, B_0 is the optical bandwidth, I_{ASE} is the photo current produced by ASE noise and I_s is the photo current produced by the optical signal, which are given by the following equations:

$$I_{ASE} = e\eta P_{ASE}\lambda_s/hc \qquad (6)$$

$$I_s = 2e\eta P_s\lambda_s/hc \qquad (7)$$

Here e is the electronic charge, η is the detection quantum efficiency, λ_s is the laser operating wavelength, h is the Planck constant, c is the speed of light in vacuum, P_{ASE} is the total ASE noise power and P_s is the total optical signal power.

The benefit of an optical amplifier for the system depends on the input optical power, and the gain, saturation power, and noise figure of the amplifier. An optical filter after the amplifier can reduce the effect of ASE noise for the case when spontaneous-spontaneous beat noise dominates. The effect of EDFA ASE noise will also be smaller if the system operates at a wavelength of 1.53 μm, the gain peak of the EDFA, rather than 1.55 μm.

3.5. Stimulated Brillouin Scattering

The use of optical amplifiers provides the possibility of delivering high optical power to each antenna unit. However, optical nonlinear effects impose a limit on the maximum optical power which can be transmitted over a given fibre length [17]. For envisaged mm-wave systems, it is likely that stimulated Brillouin scattering will be the dominant nonlinear mechanism. SBS causes power in the forward propagating signal, $P_c(z)$, to couple to a frequency-shifted, backward-propagating signal, $P_{SBS}(z)$.

The differential equations governing power transmission are

$$\frac{\partial P_c(z)}{\partial z} = -\alpha P_c(z) - \frac{g_b P_{SBS}(z)}{a} P_c(z) \qquad (8)$$

$$\frac{\partial P_{SBS}(z)}{\partial z} = \alpha P_{SBS}(z) - \frac{g_b P_c(z)}{a} P_{SBS}(z) \qquad (9)$$

Here α is the fibre loss, g_b is the SBS gain constant and a is the effective fibre core area. The intrinsic SBS gain spectrum is Lorentzian with full width half maximum (FWHM) bandwidth $\Delta\nu$ of $\sim$ 20 MHz. The effective gain spectrum will be equal to the convolution of the intrinsic SBS spectrum and the power spectrum of the signal. SBS

limits the optical power of a narrow, unmodulated optical tone to $\sim$ 2 mW.

4. ELECTRO-OPTIC MIXING

In this section we discuss the operation and performance of a generation technique developed within the RACE project MODAL [18]. This technique generates a two-tone optical signal using a Mach−Zehnder modulator as an electro-optic mixer.

4.1. Principle of Operation

It is well known that the MZM has a raised-cosine intensity response. However, when biased at the point of minimum optical transmission, the response of the device on the optical field can be written

$$E_{out} = E_{in} \sin\left(\frac{\pi}{2}\frac{V}{V_\pi}\right) \qquad (10)$$

For small applied voltages, the device behaves as a linear mixer.

The response can be utilized for two-tone generation. Driving with a local oscillator signal at frequency $\frac{f_{mm}}{2}$, the output optical spectrum is given by

$$S(f) = \qquad (11)$$

$$P_0 \sum_{n=-\infty}^{\infty} J_{2n+1}^2(m)\delta\left[f - f_0 - (2n+1)\frac{f_{mm}}{2}\right]$$

Here J_n represents the Bessel function of the first kind of order n, and m is the modulation index. For modest drive powers, the spectrum is predominantly two-tone. The electrical spectrum produced by square-law photodetection is given by

$$S_{el}(f) = P_0 \sum_{n=1}^{\infty} J_{2n}^2(2m)\delta\left(f - 2n\frac{f_{mm}}{2}\right) \qquad (12)$$

demonstrating a doubling of the local oscillator frequency.

As the LO drive power is increased, the optical output power correspondingly increases, but additionally unwanted higher harmonics around the optical carrier are generated. These harmonics interact with chromatic dispersion in the fibre to produce fluctuations in the detected carrier power. If we set the allowed fluctuations with length to be ± 0.5 dB, the maximum LO power is 1.1 P_π, resulting in a 'single-sideband' optical conversion loss of 8.6 dB.

4.2. Data Imposition

As outlined above, a feature of the two-tone optical spectrum is that detected signal power is independent of fibre dispersion. When a subcarrier signal is imposed on the mm-wave carrier, it is desirable to preserve this simple spectrum. One technique to achieve this is shown in Fig. 1. The two optical tones are demultiplexed, and data is applied to only one tone using a second MZM operating at the subcarrier frequency f_{sc}. The second MZM is also biased at V_π. The result is that the subcarrier signal is mapped to a frequency $f_{mm} + f_{sc}$, together with an image

at $f_{mm} - f_{sc}$. This technique provides transparency to data format and is suitable for complex digital modulation and multi-channel transmission.
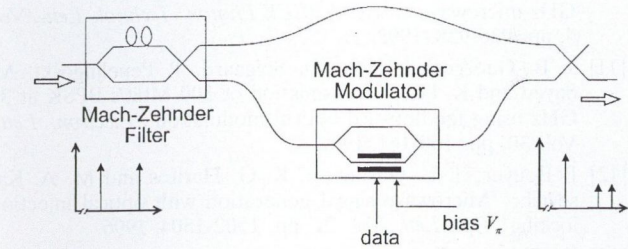

Fig. 1. Imposition of data on the optical mm-wave signal

4.3. Link Performance

To provide a measure of the performance of the mm-wave link, we have calculated the CNR for transmission as a function of fibre length. We consider the case of transmission of 10×18 Mbit/s channels using 16-QAM modulation, and impose the requirement that link CNR is sufficiently high to cause less than 1 dB degradation in the overall system power requirement for 10^{-6} BER. Component characteristics are given in Table 1, based on commercially-available devices. Although a range of different parameters and link requirements may be necessary in practice, we aim to estimate achievable performance and identify the main degradations.
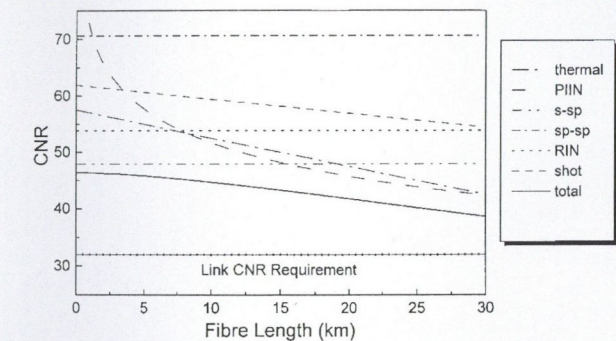

Fig. 2. Carrier-to-noise ratio for signal transmission

The results are given in Fig. 2 indicating that this scheme performs well, achieving the required CNR over lengths of fibre up to 30 km. Signal-spontaneous beat noise, receiver thermal noise and PIIN are the main sources of degradation.

Table 1. Component parameters used for analysis

Laser Output Power	5 mW
RIN	-135 dB/Hz
Laser Linewidth	5 MHz
Wavelength	1550 nm
Fibre Loss	0.25 dB/km
Dispersion	17 ps/nm.km
Carrier Frequency	30 GHz
Subcarrier Frequency	1.5 GHz
MZM1 Insertion Loss	4 dB
MZM1 LO Power	1.1 P_π
Optical Filter Loss	2 dB
MZM2 Insertion Loss	4 dB
MZM2 Drive Power	0.28 P_π
EDFA Gain	30 dB
EDFA Saturated Output	17 dBm
EDFA Noise Figure	5 dB
1×16 Insertion Loss	14.5 dB
PD Responsivity	0.5 A/W
Receiver Noise Figure	4 dB

5. CONCLUSION

Although there are many options available for the generation of optical mm-wave signals, only a limited number are appropriate to provide photonic transport in a broadband access network. We have focused on an approach using a Mach−Zehnder modulator biased for nonlinear response. The feature of dispersion tolerance makes this approach very flexible, allowing use of standard fibre at 1550 nm, and the potential for operation at higher carrier frequencies. We have identified the main impairments for system operation, and have shown that current devices will allow construction of a high performance system.

6. ACKNOWLEDGMENTS

REFERENCES

[1] J. O'Reilly and P. Lane: "Remote delivery of video services using mm-waves and optics", *J. Lightwave Technol.*, Vol. 12, pp. 369-375, 1994.

[2] O. Kjebon, R. Schatz, S. Lourdudoss, S. Nilsson, B. Stalnacke and L. Backbom: "30 GHz direct modulation bandwidth in detuned loaded InGaAsP DBR lasers at 155 mm wavelength", *Electron. Lett.*, Vol. 33, pp. 488-489. 1997.

[3] S. P. Yeung, J. B. Georges, D. M. Cutrer, T. Wu and K. Lau: "Millimeter-wave signal transmission using uncoated telecommunications-grade distributed feedback lasers", *OFC'96*, pp. 210-211, 1996.

[4] D. Novak and R. Tucker: "Millimeter-wave signal generation using pulsed semiconductor lasers", *Electron. Lett.*, Vol. 30, pp. 1430-1431, 1994.

[5] K. Y. Lau: "Short pulse and high-frequency signal generation in semicoductor lasers", *J. Lightwave Technol.*, Vol. LT-7, pp. 400-419, 1989.

[6] N. G. Walker, D. Wake and I. C. Smith: "Efficient millimeter-wave signal generation through FM-IM conversion in dispersive optical fibre links", *Electron. Lett.*, Vol. 28, pp. 2027-2028, 1992.

[7] J. J. O'Reilly, P. M. Lane, R. Heidemann and R. Hofstetter: "Optical generation of very narrow linewidth millimeter-wave signals", *Electron. Lett.*, Vol. 28, pp. 2309-2311, 1992.

[8] T. Young, J. Conradi and W. R. Tinga: "Generation and transmission of FM and DQPSK signals at microwave frequencies using harmonic generation and optoelectronic mixing in Mach−Zehnder modulators", *IEEE MTT*, Vol. 44, pp. 446-453, 1996.

[9] D. G. Moodie, D. Wake, N. G. Walker and D. Nesset: "Efficient harmonic generation using electroabsorbtion modulator", *IEEE Phot. Technol. Lett.*, Vol. 7, pp. 312-314, 1995.

[10] U. Gliese, T. N. Nielson, M. Bruun, E. L. Christensen, K. E. Stubkjaer, S. Lindgren and B. Broberg: "A wideband heterodyne optical phase-locked loop for generation of 3-18 GHz microwave carriers", *IEEE Photon. Technol. Lett.*, Vol. 4, pp. 936-938, 1992.

[11] J. B. Georges, J. Park, O. Solgaard, P. Pepeljugoski, M. Sayed and K. Lau: "Transmission of 300 Mbit/s BPSK at 39 GHz using feedforward optical modulation", *Electron. Lett.*, Vol. 30, pp. 160-161, 1994.

[12] P. Bouyer, T. L. Gustavson, K. G. Haritos and M. A. Kasevich: "Microwave signal generation with optical injection locking", *Opt. Lett.*, Vol. 21, pp. 1502-1504, 1996.

[13] D. Wake, C. R. Lima and P. A. Davies: "Transmission of 60 GHz signals over 100 km of optical fiber using a dual-mode semiconductor laser source", *IEEE Phot. Technol. Lett.*, Vol. 8, pp. 978-980, 1996.

[14] P. V. Mamyshev, S. V. Chernikov and E. M. Dianov: "Generation of fundamental soliton trains for high-bit-rate optical fiber communication lines", *IEEE J. Quantum Electron*, Vol. 27, pp. 2347-2355, 1991.

[15] W. H. Hatton and M. Nishimura: "Temperature dependence of chromatic dispersion in single mode fibres", *J. Lightwave Technol.*, Vol. 4, pp. 1552-1555, 1986.

[16] C. R. Giles and E. Desurvire: "Propagation of Signal and Noise in Concatenated Erbium-Doped Fibre Optical Amplifiers", *J. Lightwave Technol.*, Vol. 9, pp. 147-152, 1991.

[17] Y. Aoki, K. Tajima and I. Mito: "Input power limits of single-mode optical fibers due to stimulated Brillouin scattering in optical communication systems", *J. Lightwave Technol.*, Vol. 6, pp. 710-719, 1988.

[18] *R2005-ALC-SEL-DR-P-031-b1*, MODAL final report.

Robert A. Griffin received the B.Sc. degree in physics from the University of New England, Australia, in 1986, and the Ph.D. degree from the University of Kent, United Kingdom, in 1994. After graduation he worked in industry for several years. He was engaged in the development of optical fibre devices and interferometric sensors. He joined the Physics Laboratory at the University of Kent as a Research fellow in 1990. He was involved there in the development of new approaches to photonic code-division multiple access. He is currently a Research Fellow in the Department of Electronic and Electrical Engineering, University College London, where he is working on optical millimeter-wave generation and transmission for fibre/radio access.

GENERATION OF HIGH REPETITION RATE OPTICAL PULSE TRAINS USING FREQUENCY QUADRUPLING IN A HARMONICALLY MODE-LOCKED FIBER RING LASER

K. K. GUPTA   and   D. NOVAK

AUSTRALIAN PHOTONICS COOPERATIVE RESEARCH CENTRE
PHOTONICS RESEARCH LABORATORY
DEPARTMENT OF ELECTRICAL AND ELECTRONIC ENGINEERING
UNIVERSITY OF MELBOURNE
PARKVILLE VIC 3052, AUSTRALIA

We present a novel technique for the generation of optical pulse trains with millimeter-wave repetition frequency. Our method uses the nonlinear properties of a Mach–Zehnder intensity modulator to quadruple the pulse repetition frequency in an actively mode-locked erbium-doped fiber ring laser. We have generated stable optical pulse trains with repetition rates of 8 GHz and 32 GHz using RF drive frequencies applied to the modulator of 2 GHz and 8 GHz, respectively. Out technique avoids costly high speed modulators and the limitations of high frequency drive electronics and we demonstrate the potential of this method to generate low jitter millimeter-wave repetition rate optical pulse trains for future ultra-high-bit-rate optical time-division multiplexed communication systems.

1. INTRODUCTION

There is much interest in the generation of short optical pulses at very high repetition rates for future high-speed optical time division multiplexed communication networks [1]. Mode-locked fiber ring lasers are an attractive source for the generation of such short optical pulses due to their waveguide structure and easy assembly. Although passively mode-locked fiber ring lasers have been demonstrated for the generation of very short optical pulses [2]–[4], the resulting pulse trains are inherently unstable exhibiting large amplitude fluctuations and timing jitter. In addition, the achievable pulse repetition rate in passively mode-locked erbium-doped fiber ring lasers has been limited to 2 GHz [5]. In contrast, the actively mode-locked fiber ring laser can provide stable, transform-limited, picosecond optical pulses at high repetition rates with low timing jitter. In fiber ring lasers employing an external intensity modulator as the mode-locking element, harmonic mode-locking is typically implemented to achieve the generation of high repetition rate pulse trains [6]–[8]. Here an RF drive signal which is a harmonic of the laser cavity frequency is applied to the RF port of the modulator, generating optical pulses in the cavity at a repetition rate equal to the RF drive frequency. Repetition rates up to 14 GHz have been demonstrated in such ring lasers [8]. In a harmonically mode-locked fiber ring laser, the maximum pulse repetition rate is therefore limited by the modulator bandwidth as well as the drive electronics. Increasing the repetition rate requires more

costly components and high speed modulators also incur additional insertion loss and larger switching voltages [9].

Previously it has been shown that the intensity modulator in the actively mode-locked fiber ring laser could be biased appropriately in order to generate optical pulse trains with repetition frequency twice that of the drive signal frequency [10]–[12]. The requirement for ultrahigh bandwidth modulators in order to achieve millimeter-wave pulse repetition rates is thus relaxed [11], [12]. In the experiment described in [12], a LiNbO$_3$ Mach–Zehnder intensity modulator with 20 GHz bandwidth was biased at the point of minimum transmission and a 40 GHz repetition rate pulse train was generated. More recently, the generation of fourth harmonic frequencies using external modulators with appropriate biasing has been described [13], [14]. This scheme has been investigated for the generation of low phase-noise high frequency RF signals for application in microwave and millimeter-wave optical fiber transmission systems. Frequency quadrupling at both 420 MHz [14] and 15 GHz [13] has been demonstrated giving 1.6 GHz and 60 GHz signals, respectively.

In this paper we demonstrate the implementation of a harmonically mode-locked fiber ring laser incorporating an intensity modulator as the mode-locking element in the ring cavity which achieves 'pulse repetition frequency quadrupling' to generate very high repetition rate optical pulse trains. We first present the theory behind frequency quadrupling in intensity modulators and in Section 3. we demonstrate the generation of 8 GHz and 32 GHz pulse trains with low timing jitter, using RF drives to the modulator of 2 and 8 GHz, respectively.

2. THEORY OF FREQUENCY QUADRUPLING IN A MACH–ZEHNDER INTENSITY MODULATOR

Mach–Zehnder (MZ) intensity modulators have become key components in actively mode-locked fiber-ring lasers. In the harmonically mode-locked laser, an RF signal with frequency equal to a harmonic of the cavity resonance frequency (the inverse of the cavity round trip time) is applied to the modulator which modulates the incoming optical signal. After multiple passes through the modulator, the laser cavity modes become locked in phase and the

output of the cavity consists of short optical pulses with pulse repetition frequency equal to the modulating frequency and exhibiting very low timing jitter [6]−[8]. The MZ modulator can also generate harmonic frequencies by utilizing its nonlinear transfer characteristic and when biased appropriately, can both double and quadruple the input signal frequency [10]−[14].

We consider an optical signal of amplitude A, and angular frequency ω_0 modulated by an intensity modulator driven by an RF signal of amplitude V_{ac} and angular frequency ω_m. When the intensity modulator is biased at V_b, with switching voltage V_π, the total input voltage $v(t)$ applied to the intensity modulator is:

$$\nu(t) = V_\pi \beta + \alpha V_\pi \cos(\omega_m t) \qquad (1)$$

where $\beta = \frac{V_b}{V_\pi}$ is the normalized bias point of the modulator, and $\alpha = \frac{V_{ac}}{V_\pi}$ is the normalized amplitude of the modulating signal. The corresponding output electric field from the modulator will then [15] be:

$$E(t) = A \cos \left[\beta \frac{\pi}{2} + \alpha \frac{\pi}{2} \cos(\omega_m t) \right] \cos(\omega_0 t) \qquad (2)$$

For the MZ modulator described by Eqns. 1 and 2, a bias voltage of $V_b = 0$ corresponds to a transmission peak in the modulator transfer characteristic.

The Fourier transform of the output electric field using Bessel's function expansion is:

$$E(t) = J_0 \left(\alpha \frac{\pi}{2} \right) \cos \left[\beta \frac{\pi}{2} \right] \cos(\omega_0 t) -$$

$$J_1 \left(\alpha \frac{\pi}{2} \right) \sin \left[\beta \frac{\pi}{2} \right] \cos(\omega_0 t \pm \omega_m t) - \qquad (3)$$

$$J_2 \left(\alpha \frac{\pi}{2} \right) \cos \left[\beta \frac{\pi}{2} \right] \cos(\omega_0 t \pm 2\omega_m t) + \ldots$$

where the J_0 term represents the optical carrier, and J_1 and J_2 correspond to the first- and second-order modes in the optical spectrum.

When the modulator is biased at its transmission peak, $\beta = 0$ and all odd order harmonics are suppressed. Eqn. 3 then becomes:

$$E(t) = J_0 \left(\alpha \frac{\pi}{2} \right) \cos(\omega_0 t) -$$

$$J_2 \left(\alpha \frac{\pi}{2} \right) \cos \left[\beta \frac{\pi}{2} \right] \cos(\omega_0 t \pm 2\omega_m t) + \ldots \qquad (4)$$

Eqn. 4 shows that by selecting $\alpha = \frac{2}{\pi} \times 2.4048$ the optical carrier i.e. $J_0(\alpha \frac{\pi}{2}) = 0$, and the second order sidemodes at $\omega_0 \pm 2\omega_m$, become dominant. After detection with a high-speed photodiode, the RF spectrum will therefore consist of an electrical signal at frequency $4\omega_m/2\pi$, the 4th harmonic of the drive signal. Note that higher order even harmonics have been neglected in the analysis presented in Eqns. 1−4.

3. EXPERIMENT AND RESULTS

Fig. 1 shows the experimental setup of the harmonically mode-locked fiber ring laser incorporating pulse repetition frequency quadrupling. The laser consists of 15 m of Er^{3+} doped fiber as the active medium which is pumped by 67 mW of optical power at 980 nm via a WDM coupler. Isolators at the input and output of the gain

medium prevent back reflections into the pump signal. Wavelength tuning was achieved using an angled tuned etalon filter with a 3 dB bandwidth of 3 nm at 1550 nm. Mode-locking was induced by incorporating a 3 GHz MZ LiNbO$_3$ intensity modulator into the cavity. An isolator inside the cavity ensures unidirectional propagation of light in the ring cavity and a polarization controller maintains the correct polarization state of the modes travelling in the cavity. The output from the ring laser is taken via an asymmetric coupler which reflects 90 % of the light back into the cavity. From the detected optical signal from the cavity observed on a spectrum analyzer, the overall ring cavity length was calculated as 29 m corresponding to the measured cavity resonance frequency of 7.11 MHz. For mode-locking and pulse generation, a synthesized RF generator provides the drive signal which is amplified using a high power amplifier before being applied to the RF port of the MZ modulator. A DC-4.2 GHz bandwidth amplifier was used for 8 GHz pulse generation and a 6−18 GHz amplifier for 32 GHz pulse generation.
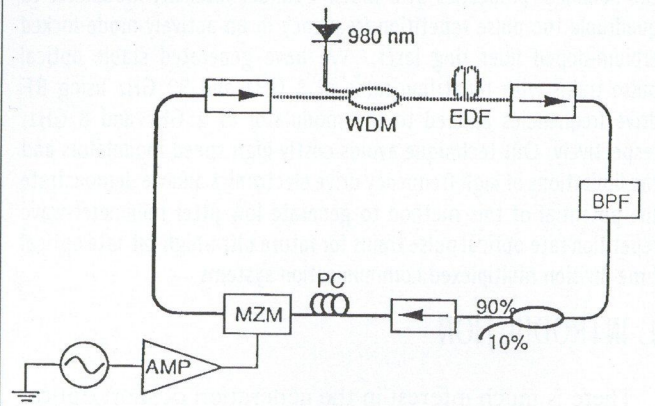

Fig. 1. Experimental setup of active harmonically mode-locked fiber ring laser

Harmonic mode-locking of the fiber ring cavity was first achieved by driving the modulator with an RF signal at 2.001 GHz corresponding to the 281st harmonic of the cavity resonance frequency. The intensity modulator was biased at its maximum transmission point and the drive signal power was +27 dBm. Fig. 2 shows the resulting optical pulse train at a repetition frequency of 8 GHz, as measured using a Tektronix CSA803 Signal Analyzer in conjunction with a 45 GHz bandwidth photodiode. The risetime of the sampling head used in this measurement was 17.5 ps. The corresponding optical spectrum was observed on an optical spectrum analyzer with minimum resolution of 0.1 nm and is shown in Fig. 3. Assuming a sec^{2}h pulse shape, the FWHM pulsewidth measured with a SHG autocorrelator was 13.48 ps. A high speed pin photodiode with 45 GHz bandwidth in conjunction with a 40 GHz spectrum analyzer was used to measure the RF spectrum of the 8 GHz optical pulse train and is shown in Fig. 4. Fig. 4 shows that the 2nd harmonic of the drive signal at 4 GHz was suppressed by 32 dB below the power in the 4th harmonic at 8 GHz. The second harmonic frequency component could have been further reduced by applying a larger RF drive signal power level however our drive electronics limited the maximum RF

power applied to the modulator to +27 dBm. Inserting the measured switching voltage and bias values for the intensity modulator in Eqn. 1 gave a calculated required RF power to the modulator of +30 dBm to fully suppress the carrier and odd order harmonic components.
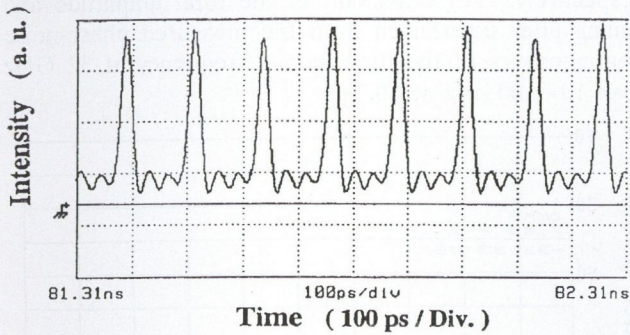

Fig. 2. Oscilloscope trace of optical pulse train at 8 GHz repetition rate using frequency quadrupling in fiber ring laser
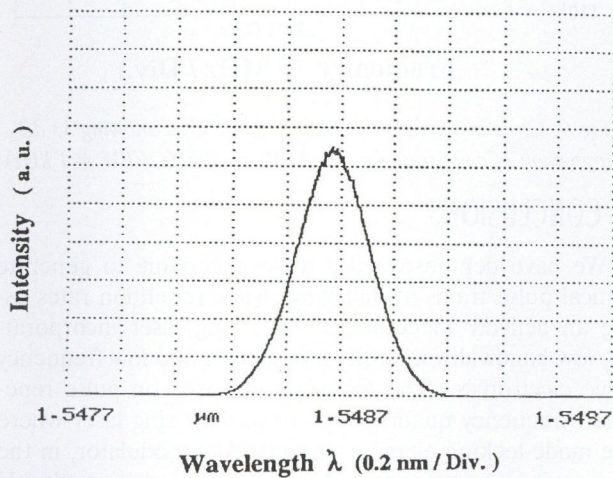

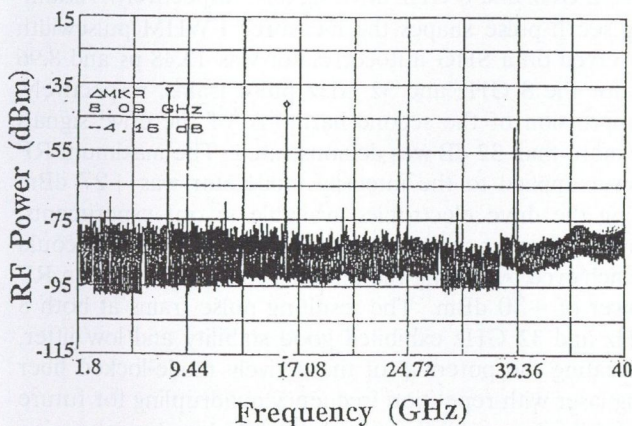*Fig. 3. Measured optical spectrum of 8 GHz optical pulse train (RBW = 0.1 nm)*

Fig. 4. Measured RF spectrum of 8 GHz optical pulse train (RBW = 300 kHz, VBW = 10 kHz)

Fig. 5 shows a close-in view at 8 GHz of the measured RF spectrum of the 8 GHz optical pulse train. Suppression of the cavity resonance modes by 42 dB below the main mode confirms the stability of the ring laser. The

single side-band phase-noise of the fundamental frequency component in the RF spectrum of the detected 8 GHz pulse train was measured as −87 dBc/Hz at 10 kHz offset and −95 dBc/Hz at 100 kHz offset frequency from the carrier. For comparison, the measured phase-noise of the 2 GHz synthesizer signal was −91 dBc/Hz and −112.2 dBc/Hz at 10 kHz and 100 kHz offsets, respectively. The low phase-noise of the 8 GHz pulse train shows that the optical pulses exhibit low timing jitter. The measured phase-noise includes contributions from both timing jitter (phase noise) and amplitude fluctuations (amplitude noise). Typically, the rms timing jitter is calculated from the measured phase-noise at large harmonic numbers where timing jitter is dominant [16] however in our experiment, only the 4th harmonic of the 8 GHz could be observed. An estimate of the total jitter calculated from the measured phase-noise was 0.3 ps.
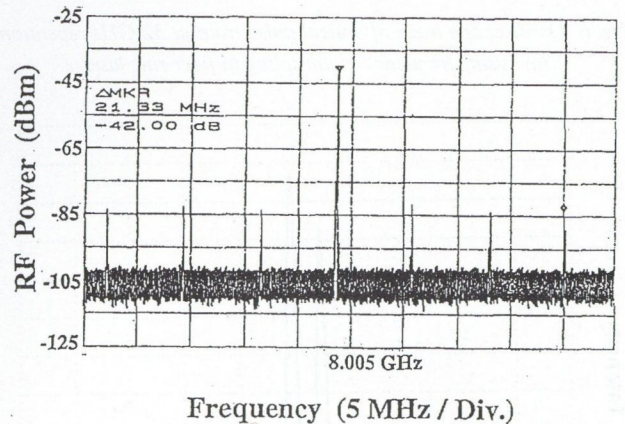

Fig. 5. Close-in view of RF spectrum at 8 GHz showing 42 dB suppression of cavity resonances (RBW = 10 kHz, VBW = 1 kHz)

In the second implementation of the harmonically mode-locked fiber ring laser, a 12 GHz intensity modulator was inserted in the cavity in order to demonstrate pulse repetition frequency quadrupling to generate millimeter-wave repetition rate optical pulse trains. The experimental setup is identical to that shown in Fig. 1 with a cavity resonance frequency of 7.83 MHz being measured (due to the slightly shorter cavity length with the different modulator). The fiber ring laser was harmonically mode-locked by applying an electrical signal to the modulator at 8.003 GHz, corresponding to the 1022nd harmonic of the cavity resonance frequency, with +27 dBm of RF power. The modulator was biased at its maximum transmission point to generate frequency quadrupling and the resulting optical pulse train at a repetition rate of 32 GHz was observed on the Tektronix CSA803 Signal Analyzer as shown in Fig. 6. The FWHM pulsewidth as measured on a SHG autocorrelator was 8.96 ps assuming a sec^{2}h pulse shape.

Fig. 7 shows the corresponding optical spectrum which consists of several optical modes separated by 0.25 nm, confirming the pulse repetition rate of 32 GHz at $\lambda = 1548$ nm. The RF spectrum of the 32 GHz optical pulse train was detected using a 45 GHz bandwidth photodiode and observed on a millimeter-wave spectrum analyzer, as shown in Fig. 8. Greater than 25 dB suppression of the second harmonic of the drive signal at 16 GHz was

achieved. Harmonic frequencies of the 32 GHz repetition frequency could not be measured due to the bandwidth limitations of the mm-wave photodetector and spectrum analyzer.
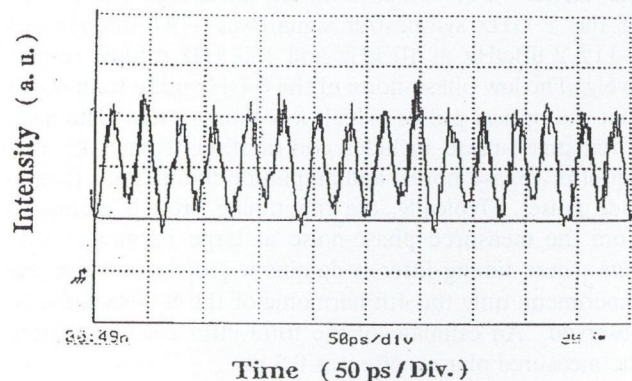

Fig. 6. Oscilloscope trace of optical pulse train at 32 GHz repetition rate using frequency quadrupling in fiber ring laser
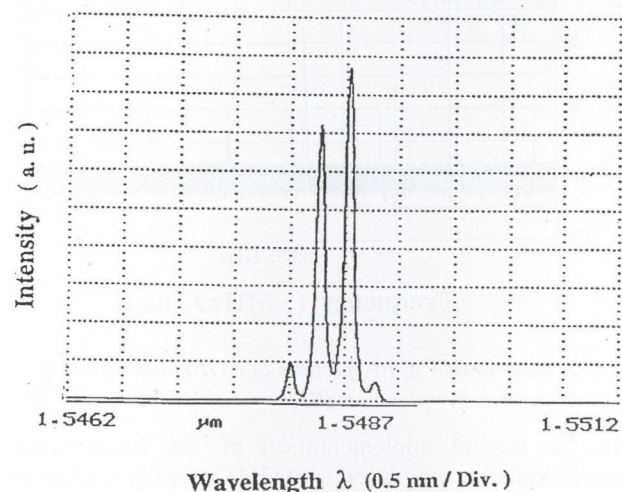

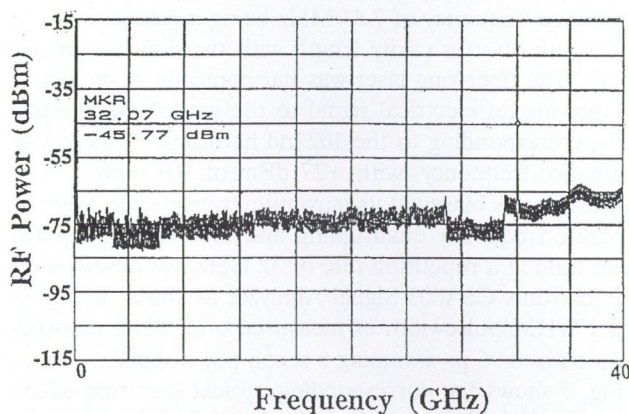*Fig. 7. Measured optical spectrum of 32 GHz optical pulse train (RBW = 0.1 nm)*

Fig. 8. Measured RF spectrum of 32 GHz optical pulse train (RBW = 300 kHz, VBW = 10 kHz)

Fig. 9 shows the close-in view of the 32 GHz repetition frequency with 33 dB suppression of the cavity modes observed. The measured phase-noise of the 32 GHz signal was −76.66 dBc/Hz and −90.74 dBc/Hz at 10 kHz and 100 kHz offset frequency from the carrier signal, respectively. An estimation of the total amplitude and timing jitter determined from the measured phase-noise characteristics of the fundamental frequency at 32 GHz over 10−100 kHz was 0.2 ps.
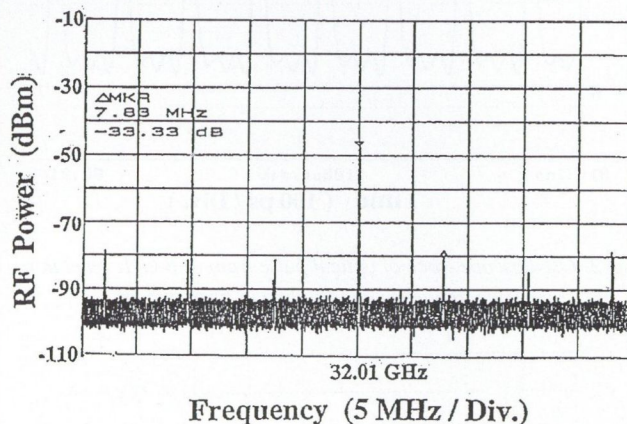

Fig. 9. Close-in view of RF spectrum at 32 GHz showing 33 dB suppression of cavity resonances (RBW = 10 kHz, VBW = 1 kHz)

4. CONCLUSIONS

We have demonstrated a novel technique to generate optical pulse trains at millimeter-wave repetition rates using an actively mode-locked fiber ring laser incorporating low bandwidth intensity modulators and low frequency drive electronics. The technique is based on pulse repetition frequency quadrupling in the fiber ring laser where the mode-locking element, the intensity modulator, in the ring cavity is appropriately driven and biased to quadruple the RF drive frequency. For the first time we have demonstrated the generation of optical pulse trains at 8 GHz and 32 GHz repetition rates by driving an intensity modulator with 2 GHz and 8 GHz drive signals, respectively. Assuming $\sec^2 h$ pulse shapes the measured FWHM pulsewidth observed on a SHG autocorrelator was 13.48 ps and 8.96 ps for the 8 GHz and 32 GHz pulse trains, respectively. Suppression of the second harmonic of the drive signals by more than 32 dB was demonstrated. The maximum RF power applied to the intensity modulator was +27 dBm using the drive electronics available in out experiments, however further suppression of the second harmonic could be achieved by driving the intensity modulator with an RF power of +30 dBm. The resulting pulse trains at both 8 GHz and 32 GHz exhibited good stability and low jitter, indicating the potential of the actively mode-locked fiber ring laser with repetition frequency quadrupling for future high-bit-rate optical time-division multiplexed transmission systems.

5. ACKNOWLEDGMENT

REFERENCES

[1] R. S. Tucker, G. Eisenstein and S. K. Krotoky: "Optical time-division multiplexing for very high-bit rate systems", *Proc. CLEO*, paper TUK5, Anaheim, CA, 1988.

[2] M. Zirngibl, L. W. Stulz, J. Stone, J. Hugi, D. Digiovanni and P. B. Hansen: "1.2 ps pulses from passively mode-locked laser diode pumped Er-doped fiber ring laser" *Electron. Lett.*, Vol. 27, pp. 1734-1735, 1991.

[3] I. N. Daling: "Subpicosecond alt-fiber erbium laser", *Electron. Lett.*, Vol. 27, pp. 544-545, 1991.

[4] H. A. Hause, E. P. Ippen and K. Tamura: "Additive pulse mode-locking in fiber lasers", *IEEE J. Quantum Electron.*, Vol. 30, No. 1, pp. 200-208, Jan. 1994.

[5] S. J. Frisken, C. A. Telford, R. A. Betts and P. S. Atherton: "Passively mode-locked erbium-doped fiber laser with nonlinear fiber mirror", *Electron. Lett.*, Vol. 27, pp 887- 889, 1991.

[6] X. Shan, D. Cleland and A. Ellis: "Stabilising Er-fiber soliton laser with pulse phase locking", *Electron. Lett.*, Vol. 28, pp. 182-183, 1992.

[7] G. T. Harvey and L. F. Mollenauer: "Harmonically mode-locked fiber ring laser with an internal Fabry-Perot stabilizer for soliton transmission", *Opt. Lett.*, Vol. 18, pp. 107-109, 1993.

[8] R. P. Davey, K. Smith and A. McGuire: "High speed, mode-locked, tunable, integrated erbium fiber laser", *Electron. Lett.*, Vol. 28, pp. 482-483, 1992.

[9] G. K. Gopalkrishanan, C. H. Bulmer, W. K. Burns, R. W. McElhanon and A. S. Greenblatt: "40 GHz, low halt wave voltage Ti:LiNbO$_3$ intensity modulator", Electron. Lett:, Vol. 28, pp. 826-827, 1992.

[10] H. Tokara, S. Kawanishi, M. Saruwatari and K. Noguchi: "Generation of highly stable 20 GHz transform-limited optical pulses from actively mode-locked Er^{3+}-doped fiber lasers with an all-polarization maintaining ring cavity", *Electron. Lett.*, Vol. 28, pp. 2095-2096, 1992.

[11] A. Takada and H. Miyazawa: "30 GHz picosecond pulse generation from actively mode-locked erbium-doped fiber laser", *Electron. Lett.*, Vol. 26, pp. 216-217, Feb. 1990.

[12] Th. Pfeiffer and G. Veith: "40 GHz pulse generation using a widely tunable alt polarization preserving erbium fiber ring laser", *Electron. Lett.*, Vol. 29, pp. 1849- 1850, 1993.

[13] J. J. O'Reilly and P. M. Lene: "Fibre-supported optical generation and delivery of 60 GHz signals", *Electron. Lett.*, Vol. 30, pp. 1329-1330, 1994.

[14] Ali Motamedi and R. Vahldiek: "Generation of 4th harmonic microwave signals using Mach−Zehnder modulators", *Proc. OFC'97*, paper FDI, Dallas, TX, 1997.

[15] H. Schmuck: "Comparison of optical millimeter-wave system concepts with regard to chromatic dispersion", *Electron. Lett.*, Vol. 31, pp. 1848-1849, 1995.

[16] D. Von der Linde: "Characterization of the noise in continuously operating mode-locked laser", *Appl. Phys. B*, Vol. 39, pp. 201-217, 1986.

Kamal K. Gupta received his M.Sc. degree in Electronics in 1986 and M.Tech. degree in Microwave Electronics in 1988, both from the University of Delhi, India. From 1989 to 1991 he worked as an Assistant Manager (R&D) at Rajasthan Communications Ltd., India. In 1992, he was appointed as Research Assistant at the School of Microelectronic Engineering, Griffith University, Brisbane, Australia. He is currently pursuing a Ph.D. degree in the Department of Electrical and Electronic Engineering, University of Melbourne, Melbourne, Australia. His research interests include fiber-compatible optical sources for microwave and millimeter-wave signal generation, with special emphasis on the short-pulse generation at millimeter-wave repetition rates from actively mode-locked erbium doped fiber ring lasers.

Dalma Novak graduated from the University of Queensland, Australia, in 1987 receiving the degree of Bachelor of Engineering (Electrical) with First Class Honours. She received the Ph.D. degree from the same university in 1992. Her Ph.D. project investigated the dynamic behaviour of directly modulated semiconductor lasers. In September 1992 she joined the Photonics Research Laboratory (PRL) in the Department of Electrical and Electronic Engineering at the University of Melbourne where she is now a senior lecturer. The PRL is a member of the Australian Photonics Cooperative Research Centre and she manages the Centre Project on Fiber-Optic Wireless Systems. Her research interests include fiber-optic wireless systems and high-speed optical communication networks.

NONLINEAR TRAVELLING WAVE PHOTODETECTOR FOR MILLIMETER-WAVE HARMONIC FREQUENCY GENERATION

I. V. RYJENKOVA, M. ALLES and D. JÄGER

FACHGEBIET OPTOELEKTRONIK, SONDERFORSCHUNGSBEREICH 254
GERHARD-MERCATOR-UNIVERSITÄT DUISBURG
KOMMANDENTENSTRASSE 60, 47048 DUISBURG, GERMANY

In this paper, a special kind of photodetector is discussed, which is used for high power nonlinear heterodyne mixing of two optical input signals, the difference frequency being in the millimeter-wave range. For that purpose, a travelling-wave structure is considered providing an optimum opto-electric power conversion efficiency. The device further includes a periodic array of nonlinear Schottky diodes for a direct second harmonic generation of the beat frequency. Results of numerical and experimental investigations are finally presented.

1. INTRODUCTION

Recently, a growing interest has been paid to the development of high-speed travelling-wave (TW) photodetectors [1]−[3]. These devices are expected to play an important role in the development of high-speed optical communication links [4]. In contrast to lumped elements these devices can overcome the usual RC-time limits, and offer large bandwidths and high power conversion efficiencies due to their distributed structure.

On the transmitter side, the optical source has usually to provide two optical signals with a beat frequency in the desired millimeter-wave range [4], [5]. However, the problems which arise from this concept can partly be overcome by using optical signals at a much lower difference frequency and generating the required millimeter-wave frequency on the receiver side by suitable nonlinear interaction. For this purpose nonlinear transmission lines (NLTLs) can be used which offer — in a bi-modal configuration, for example — direct harmonic frequency generation with a large power conversion efficiency [6]−[9].

In this paper, we study special travelling wave photodetectors, which are monolithically integrated with an array of nonlinear varactor diodes. The device is used for a heterodyne mixing of two optical input signals and a direct conversion into second harmonic power.

2. TRAVELLING-WAVE (TW) PHOTODETECTOR

The general outline of a distributed travelling-wave photodetector is shown in Fig. 1. It consists of an electrical coplanar waveguide coupled to an optical waveguide. Here the ridge optical guide (InGaAlAs) is closely positioned to a lossy InGaAs layer where the photocarriers are generated. Further, a Schottky center contact forms a depletion layer at the metal semiconductor interface giving rise to a distributed electrical nonlinearity [10] and a

current source $\mathbf{J}'$ due to optical absorption [2], [3]. The corresponding equivalent circuit is shown in Fig. 2, cf. Refs [2], [3], [10].
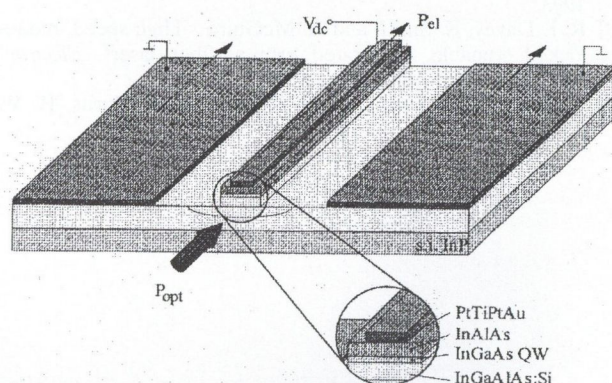

Fig. 1. Sketch of the travelling-wave photodetector, P_{opt} and P_{el} are the input optical and output electrical powers, respectively, [2], [3]
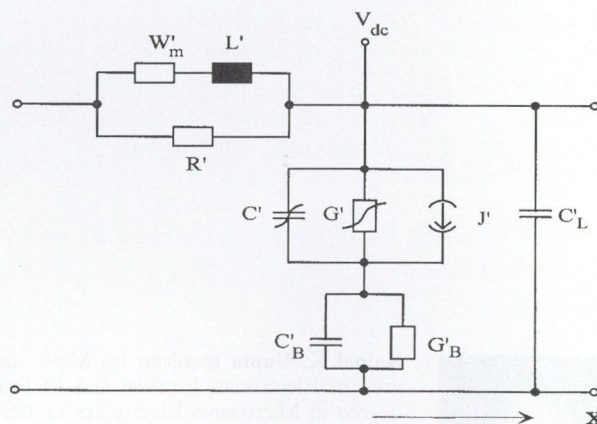

Fig. 2. Distributed electrical equivalent circuit model of the travelling-wave photodetector

It should be noted at this point, that the power conversion efficiency of the device in Fig. 1 is at an optimum under phase matching conditions, i.e. when the microwave and optical phase velocities are the same. Moreover, the nonlinearity of $\mathbf{G}'$ and especially $\mathbf{C}'$ of Fig. 2 can basically be applied for harmonic frequency generation. Here an optimum power conversion is obtained under electri-

cal phase matching conditions, which occur in bi-modal NLTLs as discussed in the following chapter.

3. BI-MODAL NLTLs

In Fig. 3, a bi-modal NLTL is shown which consists of a bi-periodic arrangement of nonlinear varactor diodes (C) and fixed capacitances (C_0). The dispersion of such a structure can be engineered in such a manner that — when using common Schottky/quantum barrier varactor diodes as nonlinear elements — the phase velocity of the second/third harmonic can be matched to that of the fundamental wave. Power conversion efficiencies of ca. 70/25 % have been predicted in the literature [6]–[9].
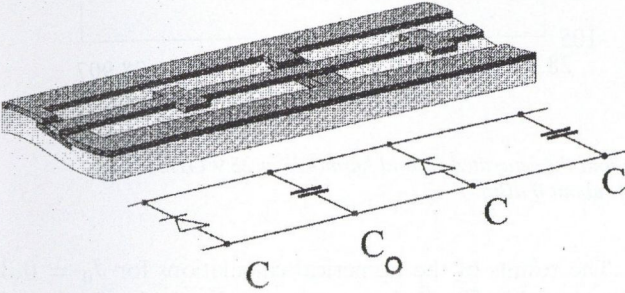
Fig. 3. Monolithic bi-modal NLTL for efficient, high-power millimeter-wave generation [6]–[9]

4. NONLINEAR TW PHOTODETECTOR

In the following, a nonlinear travelling-wave photodetector is studied where the structure of Fig. 3 is coupled to an optical waveguide as sketched in Fig. 1. Accordingly, a TW opto-electric power converter results which consists of a periodic arrangement of Schottky photodiodes alternating with fixed capacitances C_0 fabricated on the s.i. InP substrate. Hence the equivalent circuit is that of Fig. 4 where every second element consists of a nonlinear capacitance, $C(V_{k+1}) = C_0/(1 + \delta V_{k+1})$, and a current source $J_k = J_0 \exp(-\alpha k) \sin(\omega t - Bk)$. Here J_0 is given by the optical input power through

$$\sum_k < J_k > = \eta P_{opt}/(ghf), \qquad (1)$$

α is the optical absorption per section. Z_e and Z_a are the input and output loads, and P_{el} is delivered to the input load (see below). The parameters of the model line are $C_0 = 92.8 fF$, $L = 162$ pH, $R = 0.2\Omega$, $G = 0.5$ S, $\delta = 1.0$ V^{-1} and $\alpha = 1/15$.
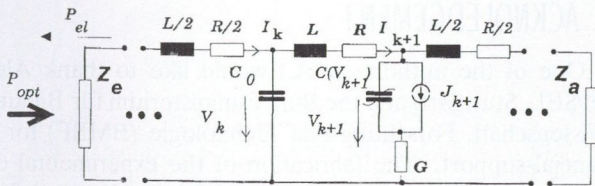

Fig. 4. Equivalent circuit of the bi-modal NLTL of Fig. 3 including the current sources J_k due to the generation of photocarriers

The dispersion relation $f(B)$ for the bi-modal NLTL

under study is shown in Fig. 5. It consists of an acoustical $(f_1(B))$ and an optical $(f_2(B))$ branch described by:

$$f_1(B) = f_c \sin(B/2) \text{ and } f_2(B) = f_c \cos(B/2). \qquad (2)$$
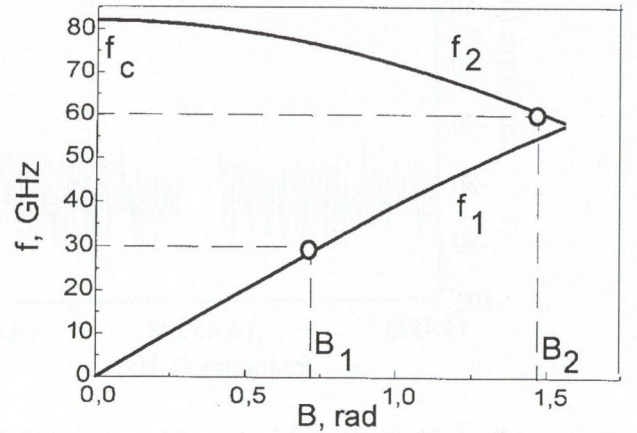

Fig. 5. Frequency vs. phase shift per section, B, of the bi-modal NLTL. Phase matching is shown by circles.

Here $f_c = 1/(\pi\sqrt{C_0 L})$ is the cut-off frequency. In order to assure phase matching conditions between the fundamental and second harmonic, $f_2 = 2f_1$, by setting $B_2 = 2B_1$ we get $f_1 = 0.36602f_c = 30$ GHz, which provides phase matching to the second harmonic at $f_2 = 60$ GHz. For numerical simulation of the nonlinear TW photodetector we use the equivalent circuit of Fig. 4 which yields the following transmission line equations:

$$LdI_k/dt = V_{k-1} - V_k - I_k R - (I_k - I_{k-1})/G, \qquad (3)$$

$$LdI_{k+1}/dt =$$
$$V_k - V_{k+1} - I_{k+1}R - (I_{k+2} - I_{k+1})/G, \qquad (4)$$

$$-C_0 dV_k/dt = I_{k+1} - I_k, \qquad (5)$$

$$-C(V_{k+1})dV_{k+1}/dt = I_{k+2} - I_{k+1} + J_{k+1}. \qquad (6)$$

5. RESULTS

The structure of the travelling-wave photodetector depicted in Fig. 1 is grown on InP-substrate for operation at 1.3 or 1.55 μm. The fabrication starts with an In-GaAlAs optical waveguide. An absorbing InGaAs layer on top of the optical waveguide is used for carrier generation. The MBE-growth is completed by an InAlAs-film as a cladding layer and an InAlAs/AlAs superlattice as a Schottky-barrier enhancement layer.

Fabricated travelling-wave photodetectors with a device length of 1 mm have been measured using a heterodyne setup at 40 GHz and an optical wavelength of 1.3 μm. As a result, an electrical output power of -19.7 dBm could be achieved for an optical input power of about 0 dBm per optical carrier at a reverse bias of 12 V.

The measured second harmonic generation of the travelling-wave photodetector is depicted in Fig. 6. Figs. 6(a) and (b) show the photo-generated fundamental mode at 14.45 GHz and the second harmonic at 28.9 GHz, respectively.
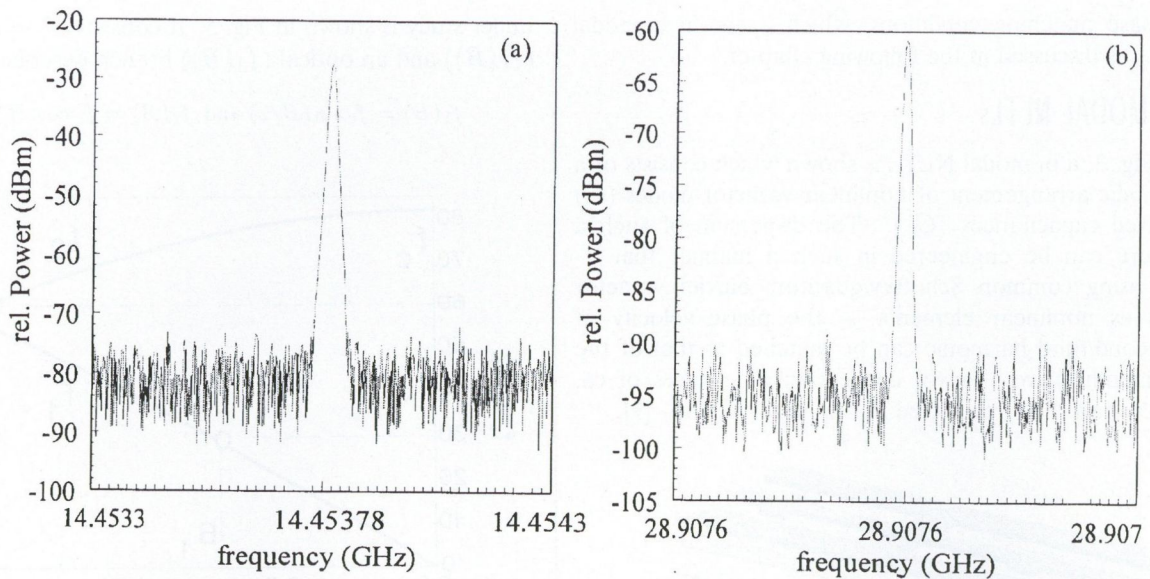
Fig. 6. Photo-generated fundamental signal at 14.45 GHz (a) and the generated second harmonic at 28.9 GHz (b). The total optical input is about 0 dBm.

As can be seen, the nonlinearity of the TW photodetector can be used to generate the second harmonic. The efficiency, however, is small due to excitation of undersized harmonics and a phase mismatch between the frequencies under study. Additionally, high attenuation causes a further reduction of the efficiency.

In the following we study the TW photodetector of Fig. 4 under phase matching conditions of Fig. 5. The numerical algorithm, based on an FFT and a Runge−Kutta four-step integrator, is developed to solve the initial-boundary-value problem of the ordinary differential equations (3) to (6). The code is based on an object oriented approach to describe the fundamental properties of the TW photodetector.
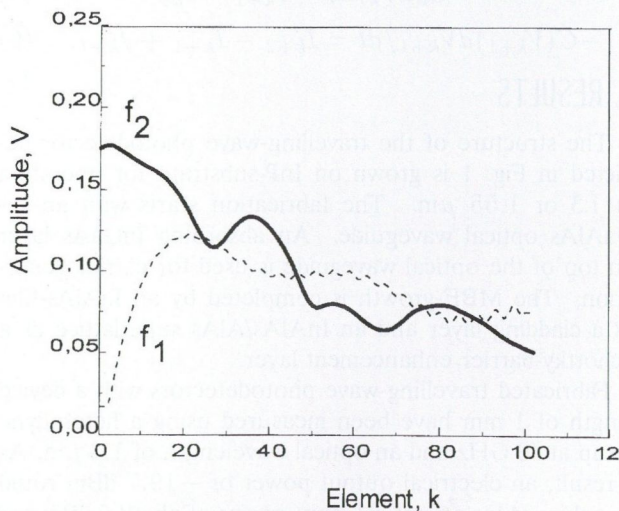

Fig. 7. Spatial distribution of fundamental (f_1) and second harmonic (f_2) amplitude

The results of the numerical calculations for $J_0 = 0.3$ are plotted in Fig. 7 showing the amplitude distribution of the fundamental and second harmonic wave. As can be seen, there is an increase of optically generated millimeter-wave at f_1 in the first part of the device. After reaching a maximum, due to a gradual decrease of optical power with increasing $\mathbf{k}$, the amplitude of the fundamental wave becomes now smaller. Note, that due to the dispersion from Fig. 5, the second harmonic wave has a negative group velocity. Thus the electrical power at f_2 is delivered to the input port of the device. Fig. 7 shows that the amplitude at f_2 delivered to Z_e can reach values comparable to that of the fundamental wave, pointing to an excellent power conversion efficiency.

6. CONCLUSIONS

In summary, it is shown that TW photodetectors based upon Schottky contact transmission lines can reveal a pronounced nonlinearity which is capable to produce directly the second harmonic of the optical beat frequency. When using a bi-modal electrical structure, phase matching can be achieved between the optical and the fundamental and second harmonic electrical wave thus producing high power conversion efficiencies. Experimental devices have been designed using semiconductor data of optical and coplanar electrical waveguides.

7. ACKNOLEDGEMENT

REFERENCES

[1] K. S. Giboney, R. L. Nagarajan, T. E. Reynolds, S. T. Allen, R. P. Mirin, M. J. W. Rodwell and J. E. Bowers: "Travelling-wave photodetectors with 172-GHz bandwidth and 76 GHz bandwidth-efficiency product", *IEEE Photon. Techn. Lett.*, vol. 7, pp. 412-414, 1995.

[2] M. Alles, Th. Braasch and D. Jäger: "High-speed coplanar Schottky travelling-wave photodetectors", *Proc. Topical Meeting of Integrated Photonics Research (IPR)*, Boston, USA, pp. 380-383, 1996.

[3] M. Alles, T. Braasch, R. Heinzelmann, A. Stöhr and D. Jäger: "Optoelectronic devices for microwave and millimeter-wave optical links", MIKON '96, *Workshop Optoelectronics in Microwave Technology*, Warsaw, Poland, 1996 (invited).

[4] D. Wake, C. R. Lima and P. A. Davies: "Transmission of 60 GHz signals over 100 km of optical fiber using a dual-mode semiconductor laser source", *IEEE Photon. Techn. Lett.*, vol. 8, pp. 578-580, 1996.

[5] J. J. O'Reilly, P. M. Lane, R. Heidemann and R. Hofstetter: "Optical generation of very narrow linewidth millimeter wave signals", *Electron. Lett.*, vol. 28, pp. 2309-2310, 1992.

[6] R. Hülsewede, V. K. Mezentsev, S. L. Musher, I. V. Ryjenkova, S. K. Turitsyn and D. Jäger: "Millimeter wave generation on nonlinear transmission lines", *Proc. International Workshop on Millimeter Waves*, Orvieto, Italy, pp. 181-183, 1996.

[7] R. Hülsewede, V. K. Mezentsev, I. V. Ryjenkova, S. K. Turitsyn and D. Jäger: "Travelling wave generation of millimeter waves in bi-modal NLTLs", *Proc. 26th European Microwave Conference*, Prague, Czech Rep., 1996.

[8] D. Jäger, V. K. Mezentsev, S. L. Musher and I. V. Ryjenkova: "Millimeter wave power generation on nonlinear transmission lines", *Proc. Asia Pacific Microw. Conf.*, New Delhi, India, 1996 (invited).

[9] I. V. Ryjenkova, V. K. Mezentsev, S. L. Musher, S. K. Turitsyn, R. Hülsewede and D. Jäger: "Millimeter wave generation on nonlinear transmission lines", *Ann. des Telecomm.*, Special Issue, 1996 (invited).

[10] D. Jäger: "Slow wave propagation along variable Schottky contact microstrip line", *IEEE Trans. Microwave Theory and Techn.*, vol. 24, pp. 566-573, 1976.
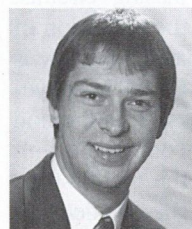
Irina V. Ryjenkova received the M. Sc. degree in applied mathematics from Novosibirsk University (Russia), in 1981 and the Ph.D. degree in optics from the Institute of Automation and Electrometry, Siberian Branch of the Russian Academy of Science in 1995. From 1988 to 1996 she was Research Scientist at the Nonlinear Physics Laboratory of Institute of Automation and Electrometry. In 1994 and 1996 she joined the Institute of Optoelectronics, Duisburg University. Her research interests include the numerical analysis of nonlinear phenomena in optics and electronics.

Dieter Jäger received the Diplom-Physiker, and the Dr. rer. nat, and the Habilitation degrees in Physics from the University of Münster. From 1974 to 1990 he has been the Head of a research group at the Institute for Applied Physics, University of Münster, where he became an Associate Professor of Physics in 1985. In 1990 he joined the Faculty of Electrical Engineering of the University of Duisburg where he is Head of the Institute of Optoelectronics.

Martin Alles received the diploma degree in electrical engineering from the university of Dortmund in 1994. Since September 1994, he is a research assistant at the institute of optoelectronics of the university of Duisburg. His research interests are the development of high-speed travelling-wave photodetectors, numerical simulations, and high-frequency measurement techniques.

OPTICALLY CONTROLLED SEMICONDUCTOR COPLANAR-STRIP WAVEGUIDE ATTENUATOR/MODULATOR: DESIGN CONSIDERATIONS

S. GEVORGIAN and E. KOLLBERG

DEPARTMENT OF MICROWAVE TECHNOLOGY
CHALMERS UNIVERSITY OF TECHNOLOGY
412 96 GOTHENBURG, SWEDEN

Design problems of optically controlled semiconductor CPS have been studied aimed to reduce consumed optical power. A quasi static field distribution and a simple models for optically induced attenuation in CPS are proposed. It is shown that optically induced attenuation as large as 10 dB/cm can be achieved in a silicon CPS with a slot width 40 μm, at frequencies above 3 GHz at 1 mW optical power.

1. INTRODUCTION

Optical control of semiconductor lumped elements (p-i-n diode [1], gap in a microstrip [2]−[4] etc.) and distributed circuit elements (microstrip, coplanar waveguide [2], [3] has been studied in the past. The main limiting factor in the performance of these devices still remain the high optical control power consumption. Little effort has been done to optimize microwave devices to meet lower optical power requirements (e.g. increased efficiency).

Coplanar type transmission lines, such as Coplanar Waveguide (CPW) [3], [4], Coplanar-Strip (CPS) [5], or slot lines seem to be more suitable from the point of view of optical control. In these lines the reduction of the illuminated slot width results in reduction of controlling light power. Although the method given in [3] is useful for calculation of optically induced attenuation in a CPW it is not flexible for the analysis and optimization of other coplanar type devices. In the following we analyze optical losses and give approximation for optically induced attenuation in asymmetric CPS. A simple procedure is proposed to optimize the CPS from the point of view of optical control.

2. DESIGN CONSIDERATIONS

2.1. Optical signal

In contrast to electrical control in optically controlled microwave devices one of the major problems is the losses of controlling optical signal in the optical "biasing" circuits. Reduction of these losses is a key issue in the reduction of controlling optical power. The optical "biasing" usually is carried out by direct illumination of the slot in the waveguide, Fig. 1a, using bulk lenses/microlenses. This method needs precise micro positioning and is not compatible with MMIC technology. The reflection from the metal strips result in optical losses which could hardly be avoided. In the best case (from the point of view of optical losses), the light spot is located in the midgap (Fig. 1a, spot 1). In the case of high speed attenuators/modulators, where the carrier lifetimes are very short and the induced plasma is limited by spot size this spot shape is not desirable. In this case due to the small lifetime the carriers do not fill the slot completely and the microwave/optical interaction length is also small (also Fig. 2). In general the light spot has a configuration shown in Fig. 1a (spot 1) and the reflection losses of the optical signal is given as:

$$L = -10 \log \left\{ 1 - 2\arcos(2g/D)/\pi + \right.$$
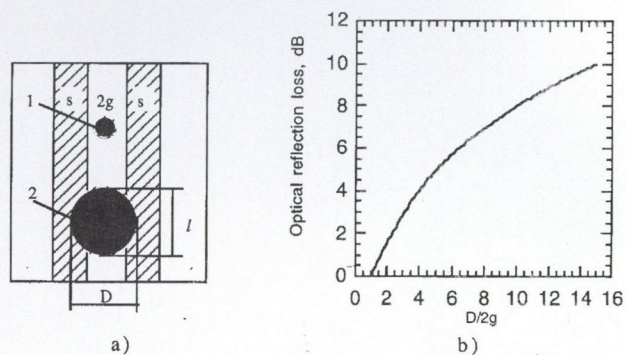$$\left. 4g[1 - (2g/D)^2]^{1/2}/(\pi D) \right\} \qquad (1)$$

Fig. 1. CPS with two configurations of optical spot (a), and the optical losses due to the reflection

The dependence of losses upon spot diameter D are shown in Fig. 1b. It follows that $L = 0$ at $D = 2g$ where the microwave/optical interaction length is also minimum, $l = D$. A further increase in the interaction length l will result in high optical loss. In practice the optical losses are limited either by extremely small gap widths or by focusing and micropositioning. Essential reduction of the optical losses and tailoring of the spot shape is possible where an Integrated Optical "biasing circuit" is used [6].

2.2. Efficiency of microwave/optical interactions

The other way to reduce controlling optical power is to increase the efficiency of microwave/optical interaction [2]. This suggests getting higher possible plasma densities at

given optical powers, which can be achieved by reducing the volume of plasma, Fig. 2c. In addition, the efficiency of microwave/optical interaction depends upon maximum overlap of the microwave field with the plasma. Both these conditions can be fulfilled by reducing the slot width, $2g$. Below we give a simple approximation for a minimum slot width using electric field and plasma distributions in CPS.
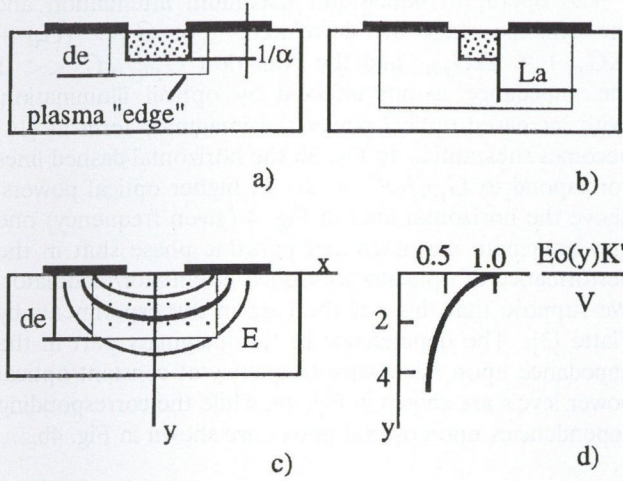

Fig. 2. Short (a) and long (b) lifetime plasma distributions, overlap of electric field and plasma (c), field distribution in x=0 plane for a 50 Ohm CPS (k=0.031)

In general the distribution of the plasma is governed by generation/recombination processes, drift and diffusion [7]. For simplicity we assume that the thickness of the plasma layer is given by: $d_e = \alpha + L_a$, where α is the optical absorption coefficient and L_a is the ambipolar diffusion length. In the devices with small carrier lifetime one has to use light spots with $D \approx 2g$, while in the case of large carrier lifetimes one can use light spots with $D < 2g$ (Fig. 1a spot 1, Fig. 2b). In the latter case due to the diffusion the plasma fills all slot width. The approximate plasmas boundaries for these two cases of illumination are shown in Fig. 2.

The electric field distribution, Fig. 2c, d, is found in a static approximation (which is valid for a quasi-TEM wave in a CPS), using conformal mapping technique:

$$E_x(y) = \frac{V}{r\,K(k')} \cos \varphi \qquad (2)$$

$$E_y(x) = \frac{V}{r\,K(k')} \sin \varphi \qquad (3)$$

$$\varphi = \frac{1}{2} \left[\tan^{-1}\left(\frac{2xy}{1-x^2-y^2} \right) + \right.$$
$$\left. \tan^{-1}\left(\frac{2k^2 xy}{1-k^2(x^2-y^2)^2} \right) \right]$$
$$r = \left\{ \left[(1-x^2-y^2)^2 + (2xy)^2 \right] \right.$$
$$\left. \left[(1-k^2(x^2-y^2))^2 \, 2k^2(xy)^2 \right] \right\}^{-1/4}$$

where $k = g/(s+g)$, $k'\sqrt{1-k^2}$, $K(k')$ is complete elliptic integral of the first kind, x and y are scaled to g, and $V = \sqrt{2Z_0 P_m}$. Here P_m is the microwave power, Z_0 is the impedance of CPS. The field distribution at $x =$

0 plane is shown in Fig. 2c. In this figure the boundaries of plasma region are also shown. For a given impedance the higher the overlap of field and plasma distributions the higher the microwave/optical interaction efficiency. From this condition we can find the optimum width of the slot. As a first approximation we take the field "penetration depth" at $y = 0$ plane, y_0, as a depth where the field decays e (=2.7128) times. This condition along with (2) and (3) gives:

$$g_{opt} = d_e/y_0 \qquad (4)$$

with

$$y_0 =$$
$$\left\{ l + k^2 + \left((1+k^2)^2 + 4k^2(e-1) \right)^{-1/2} /2k^2 \right\}^{-1/2}$$

To ensure the overlap between metal strips and plasma one should have $g < (d + L_a)$. When choosing the slot width one has to bear in mind that a reduction of the slot width causes enhancement of current crowding in the strips and higher microwave losses. Additionally this, smaller slot widths may reduce photoconductivity due to the enhanced surface recombination [8]. In this respect the determination of the lower limit of slot width may be chosen using experimental data (see for example [8].

3. OPTICALLY INDUCED ATTENUATION

The total attenuation in CPS, like in other semiconducting transmission lines, include conductor, dielectric, and conductivity losses. The losses due to the substrate conductivity are [9]:

$$\alpha_\sigma = \frac{1}{2} Z_0 G_\sigma = \frac{1}{2} Z_0 (G_d + \Delta G_{ph}) \qquad (5)$$

G_σ is the conductance of the line per unit length. The photoconductance per unit length will be addressed below. The conductance in the dark can be presented as:

$$G_d = \sigma_d \frac{K(k')}{K(k)} \qquad (6)$$

where σ_d the conductivity of the substrate in the dark, and the associated microwave losses are:

$$\alpha_d = \frac{1}{2} Z_0 G_d \qquad (7)$$

The optical illumination results in an access conductivity: $\sigma = \sigma_d + \Delta\sigma_{ph}$. The effective photoconductivity $\Delta\sigma_{ph}$ in general may be evaluated numerically. In this work we use the analytical approximation proposed in [3], [4]. For a given $\Delta\sigma_{ph}$ the optically induced attenuation may be calculated as follows:

1. $d_e >> 2g$, $g < L_a$, $\Delta G_{ph} = \Delta\sigma_{ph}\sinh^{-1}(d_e/g)$

$$\alpha_{ph} = 4.34\Delta\sigma_{ph}Z_0\sinh^{-1}(d_e/g), \text{ dB/cm} \qquad (8)$$

2. $\qquad d_e << 2g, \quad s + g < L_a,$
$$\Delta G_{ph} = \Delta\sigma_{ph}/[2(\pi g + d_e \log 4)]$$
$$\alpha_{ph} = 6.96\Delta\sigma_{ph}Z_0 d_e/(\pi g + d_e \log 4), \text{ dB/cm} \qquad (9)$$

3. $\qquad d_e << 2g, \quad g < L_a, \quad \Delta G_{ph} =$
$$\Delta\sigma_{ph}\{2g/d_e + 4[\log 2 - \log(1 - \exp(-\pi L_a/d_e))]/\pi\}^{-1}$$
$$\alpha_{ph} = 6.96\Delta\sigma_{ph}Z_0 d_e\{2g/d_e + \qquad (10)$$

$4[\log 2 - \log(1 - \exp(-\pi L_a/d_e))]/\pi\}^{-1}$, dB/cm

$$\dot{Z} \approx Z_0(1 + jG/\omega C) \qquad (11)$$

$$Z_0 = \frac{120\pi K(k)}{\sqrt{\varepsilon_e} K(k')}, \quad C = \varepsilon_e \varepsilon_0 \frac{K(k')}{K(k)}, \quad \varepsilon_e = (1+\varepsilon)/2$$

where ε is the dielectric constant of the semiconducting substrate.

4. NUMERICAL RESULTS AND DISCUSSIONS

Numerical computations are carried out for a CPS on high resistivity silicon substrate. As an example to compare with we took semiconductor parameters (and notations) given in [5]: $\varepsilon = 11.7$, $\sigma_d = 2.5 \ 10^{-4}$ (Ohm cm)$^{-1}$, $\tau = 10^{-6}$ s, $L_a = 47 \ \mu$m, $(\mu_n + \mu_p) = 2100$ (cm^2/Vs), $\nu_s = 100$ cm/s, $R = 0.3$, $\alpha = 0.07 \ \mu$m (at 0.86 μm), $s_\lambda = 1.0$. The computed effective plasma thickness, $d_e = 61.5 \ \mu$m (61.6 μm is given in [3], [4]), and computations of effective photoconductivity, $\Delta\sigma_{ph}$, is carried out using analytic approximations presented in [4]. The device (microwave/optical interaction) length $l = 10$ mm, and impedance, $Z_0 = 50$ Ohm, are kept constant in

computations. The diameter D of the light spot is assumed to be 5 μm. For computed effective plasma thickness 61.5 μm and impedance 50 Ohm the optimum dimensions of the CPS are $2g_{opt} = 5 \ \mu$m, $s_{opt} = 60.5 \ \mu$m. Theses dimensions are in the limit of $g/L_a \ll 1$, and the condition for maximum overlap of microwave field and plasma is fulfilled as a first approach.

The operation bandwidth, maximum attenuation and the dynamic range are correlated. For $G = (G_d + \Delta G_{ph}) \approx \Delta G_{ph}$, and the condition $G_{ph}/\omega C \ll 1$ the impedance is not affected by optical illumination. With increased optical power the imaginary term in (11) becomes substantial. In Fig. 3b the horizontal dashed lines correspond to $G_{ph}/\omega C = 1$. At higher optical powers, above the horizontal lines in Fig. 4 (given frequency) one may anticipate mismatch and parasitic phase shift in the performance of optically controlled attenuator/modulator. We suppose that this was the case in the experiments by Platte [3]. The dependence of the imaginary part in the impedance upon microwave frequency at constant optical power levels are shown in Fig. 4a, while the corresponding dependencies upon optical power are shown in Fig. 4b.
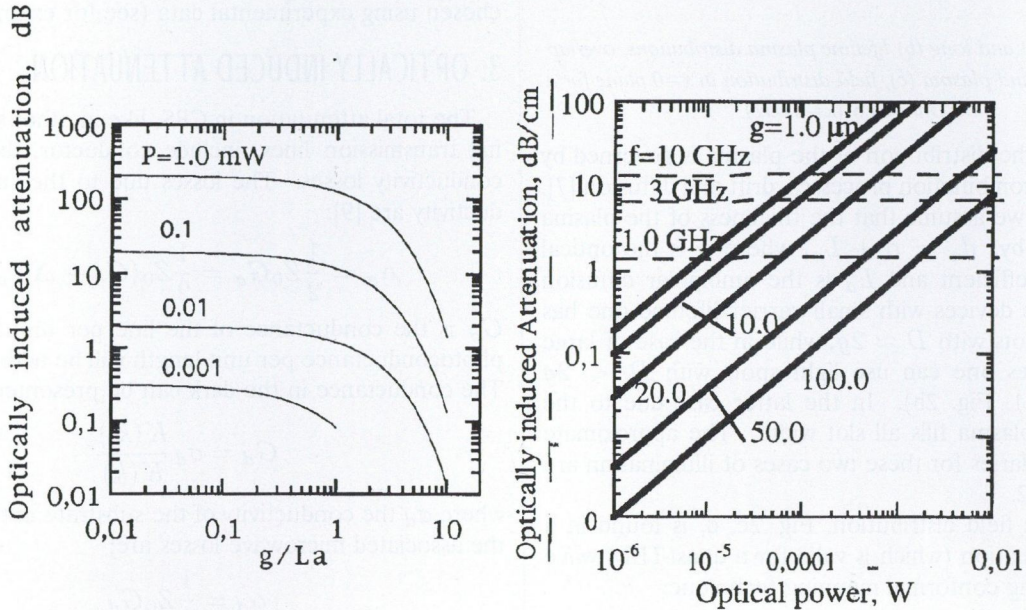
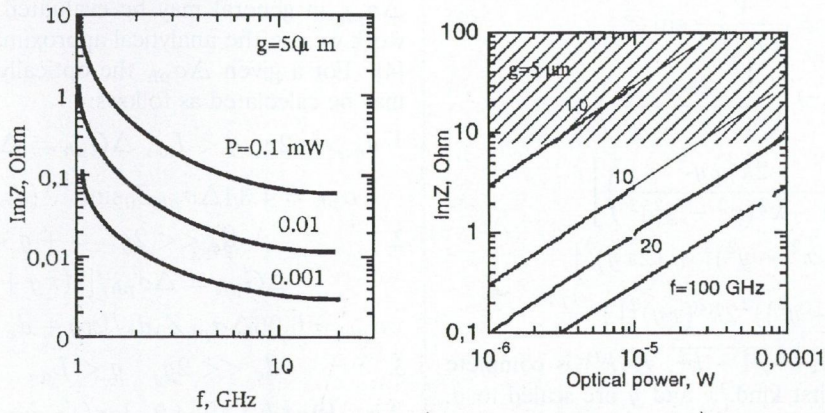*Fig. 3. Attenuation vs. slot width (a), and optical power (b)*

Fig. 4. Imaginary part of the impedance vs. frequency (a), and optical power (b)

The dependencies of optically induced microwave attentions upon slot width g are shown in Fig. 3, where the optical power is given as a parameter. For $g/L_a \leq 1.0$ the dependence is very slow, the attenuation is governed by lateral diffusion of carriers. For $g/L_a > 1.0$ the contribution from diffusion becomes negligible resulting in decreased photoconductivity and attenuation.

The dependence of the optically induced attenuation upon optical power is depicted in Fig. 3b. As it is expected the dependence is linear and large attentions can be obtained at $1-10$ mW optical powers and wide range of slot widths.

An important feature of the device is that its operation bandwidth is basically limited at lower frequencies, where the microwave frequency become comparable with plasma resonance frequency. At higher frequencies, especially in the millimeter-wave range excellent performance of the device can be obtained. The dark dielectric losses in this region are very low and high resistivity silicon is a perfect substrate material. Additionally, much larger dynamic range of optical control can be obtained at these frequencies, Fig. 3. This suggestion is particularly confirmed in a recent measurements [5].

For comparison we have computed the optically induced losses in a coplanar waveguide presented in [3]. Our results based on above formulas are 0.14 dB/cm at light intensity 30 mW/cm^2 and 1.7 dB/cm at 357 mW/cm^2 against corresponding experimental values 0.11 dB/cm and 1.35 dB/cm observed in [3].

REFERENCES

[1] P. R. Herczfeld et. al.: "Optical Control of MMIC-based Modules", *Microwave Journal*, pp. 309-321, 1988.

[2] S. Gevorgian: "Design Considerations for an Optically Exited Semiconductor Microstrip Gap at Microwave Frequencies", *IEE Proc. J.*, Vol. 139, pp. 153-157, 1992.

[3] W. Platte and B. Saurer: "Optically CW-induced Losses in Semiconductor Coplanar Waveguides", *IEEE Micr. Theory Techn.*, Vol. 37, pp. 139-149, 1989.

[4] W. Platte: "Photoduced Microwave Attenuation in LED-controlled Semiconductor Coplanar Waveguides", *AüE*, pp. 32-325, 1988.

[5] S. Gevorgian and E. L. Kollberg:"Performance of Optically Controlled Silicon Coplanar Waveguide at Cryogenic Temperatures", Dig., *International Meeting on Microwave Photonics*, Kyoto, pp. 289-292, 1996.

[6] S. Gevorgian: "Optics Control Microwaves. The Next Step", *1990 EuMC Proc.*, pp. 1603-1608.

[7] Sze S. M.: *Physics of Semiconductor Devices*, J. Wiley, N.Y., 1981.

[8] Bruce et. al.: "Surface Charge Effects on Planar Submicrometer GaAs and InP Devices", *IEEE*, ED-34, pp. 161-1616, 1987.

[9] T. C. Edwards: Fundamentals for Microstrip Circuit Design, J. Wiley, 1981.
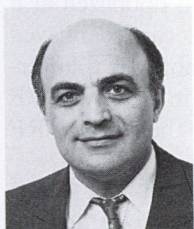
Spartak Gevorgian graduated in electronic engineering in 1972 from Engineering University of Armenia, Yerevan, and received the Ph.D. and Doctor of Science degrees from Leningrad Electrical Engineering University, S. Petersburg, Russia in 1977 and 1991, respectively. From 1977 to 1988 he was with the Engineering University of Armenia as an Associated Professor, and from 1991 to 1993 as a Professor. Since 1993 he is with the Department of Microwave Technology, Chalmers University of Technology, Sweden. His fields of interests are in Microwave Integrated Circuits, Integrated Optics, Optically Controlled Microwave Devices, and Integrated High Temperature Superconducting/Ferroelectric devices. He is the author of a book "Glass based integrated Optics", and more than 100 scientific papers.

Erik Ludvig Kollberg is a professor at School of Electrical and Computer Engineering at Chalmers University, Sweden since 1980, and was the acting Dean of Electrical and Computer Engineering 1987—1990. From 1963 to 1976 he made research on low-noise maser amplifiers used for radio astronomy observations at the Onsala Space Observatory. Since then his research has comprised low-noise millimeter-wave Schottky diode mixers, varactor diode multipliers, superconducting quasiparticle mixers, quantum well devices such as FET's and HBT's. He is the inventor of the heterostructure barrier varactor diode. In the fields mentioned above about 180 scientific papers have been published. He received the 1982 Microwave Prize given at the 12th European Microwave Conference in Helsinki, Finland, the Gustaf Dahlén gold medal 1986, and was elected Fellow of IEEE 1990. He was invited as a guest professor to École Normal Superieure, Paris, France, summer 1983/84/87. He was a visiting professor at the California Institute of Technology in 1989. He became member of the Royal Swedish Academy of Engineering Sciences 1992.

APPLICATIONS OF ANALOG FIBER-OPTIC LINKS

C. H. COX III,   E. I. ACKERMAN,   R. HELKEY   and G. E. BETTS

M.I.T. LINCOLN LABORATORY
LEXINGTON, MA, USA

This paper presents an overview of analog links based on the three major application areas: transmit, distribution and receive links.

1. INTRODUCTION

Fiber optic links are increasingly finding applications in the remoting of signals to and from cellular/personal communication systems (PCS), in the distribution of cable television (CATV) signals, and in radar antenna remoting. The wide range of application requirements and frequency ranges makes it difficult to have a general comparative discussion of the links used in all such applications. One key to organizing a comparative discussion is to recognize that fiber optic links are unidirectional, unlike the bi-directional coax or waveguide they are intended to replace. This fact often leads to emphasizing different technical requirements depending on the primary function the link is fulfilling. Consequently one way to organize a comparative discussion on links is to group fiber optic links into three functional categories: transmit, distribution and receive links.

2. TRANSMIT LINKS

A transmit link is aimed at conveying a signal from the signal source to an antenna. Applications include the up-link for cellular/PCS and the transmit function of a radar system. Since high-level signals are involved in transmit, noise figure is not a driving requirement. In radar applications, the link needs to convey only a single frequency at a time; consequently intermodulation-free dynamic range (IMFDR) is also not a driving requirement. However in the cellular/PCS up-links, multiple signals are present simultaneously, so there is the need to meet an IMFDR requirement.

Virtually all transmit applications do require a relatively high-level signal to drive the antenna. As summarized by the data in Fig. 1, most fiber optic links have significant RF-to-RF loss. In addition, the maximum RF power at the photodetector end of the link is typically on the order of −10 dBm. Consequently for an antenna to radiate 1 W means that 40 dB of gain is needed between the link output and the antenna. Further, if this link has a gain of −30 dB, then the input power to the link for −10 dBm output would be 20 dBm. This is above the 1 dB saturation power of many links, which means that a lower drive power to the link and consequently a higher-gain power amplifier after the link photodetector is required. Therefore there is a real need to decrease the loss and increase the output power capability of links for transmit applications.

The center frequency of the signal sent to the antenna can be anywhere from 10 MHz to 100 GHz. Complete links have been demonstrated up to 20 GHz. Consequently at center frequencies in this range, the transmit link is typically designed to convey the center frequency without any frequency translation.
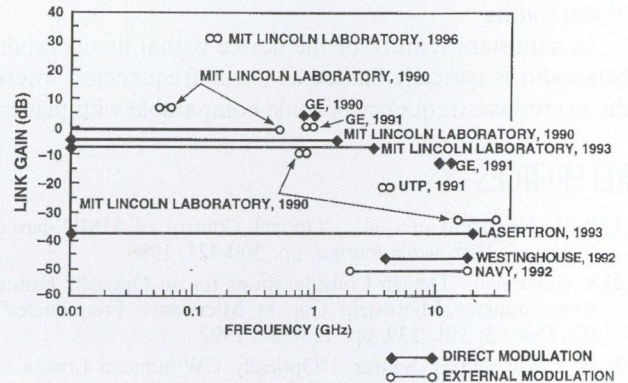

Fig. 1. Gain vs. frequency data reported for direct and external modulation links

The components necessary for higher frequency links have been demonstrated: the maximum reported bandwidth for broadband modulation of a diode laser is 33 GHz, of an external modulator is 70 GHz and of a photodetector is 500 GHz [1]−[3]. However the efficiencies of these components are such that if they were combined into a link, the intrinsic link gain would be rather low. For instance, if the 70 GHz modulator were used in a link with the 500 GHz photodetector with 1 mW of incident optical power, the gain would be approximately −60 dB at 70 GHz.

Driven primarily by the present difficulty of building broadband direct modulation links above 30 GHz and the poor performance of external modulation at higher frequencies, researchers have begun investigating links that combine transmission and frequency conversion in the same link. One approach is to send two frequencies (LO and IF) up to the photodetector, then perform the upconversion in an RF mixer [4]. This approach affords the link designer some measure of flexibility, because the performance of the LO link need only be optimized at a single high frequency, and the IF signal can be relayed with low loss or even gain and with low noise by a lower-frequency optical link. This can result in improved RF performance, especially in cases where the desired RF frequency band is exceedingly high, broad, or both.

An alternative is a frequency conversion link which uses heterodyne optical detection to generate in the photodetector the desired high frequency RF carrier, as shown in Fig. 2 [5]. In this approach the two optical carriers are offset from each other by the frequency of the RF carrier frequency that is desired. One interesting extension of heterodyne detection is that any phase shift between the optical carriers will be transformed to RF

phase shift after heterodyne detection. This feature can be used to do phase delay beam steering in a phased array.
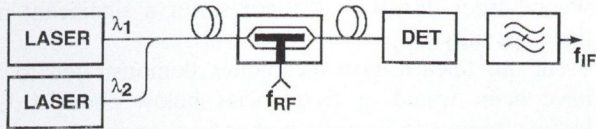

Fig. 2. Transmit link topology

3. DISTRIBUTION LINKS

This type of link is intended to distribute the same signal to a multiplicity of users. Examples of distribution links include CATV networks and phase reference distribution in a phased array radar. Like the transmit links, distribution links convey relatively high level signals, consequently link noise figure is not a driving parameter. Also like some transmit links, distribution links that broadcast the phase reference have only a single frequency present at any one time, therefore IMFDR is not a requirement.

However in other distribution applications, such as CATV, multiple frequencies are present simultaneously, so IMFDR is still a key link parameter. Further for CATV distribution, the bandwidth is generally broader than an octave, so both the second and third order IMFDR must be taken into consideration in designing links for this application.

Distribution links by their very nature have a high optical loss that is dominated by the splitting loss in the distribution network. For example, a fiber network that needs to distribute a signal to 100 locations, would have an optical splitting loss of 20 dB which translates to 40 dB of RF loss. Although the total power required is high, the power on each individual photodetector is low.

One convenient way to overcome the high splitting loss is by the use of optical amplifiers, as shown in Fig. 3. The two basic types of optical amplifiers are semiconductor [6], which are available at either of the principal fiber wavelengths, and solid state [7], which although available at either wavelength are at present only commercially viable at 1.55 μm in the form of erbium doped fibers. Either type of amplifier is capable of more than 20 dB of optical gain, but since these amplifiers have equal gain in either direction, optical reflections must be kept low in links using them. The most logical use of optical amplification to compensate for splitting loss is to insert a single optical amplifier before the optical splitter. Unfortunately the low saturation power of present optical amplifiers generally rules out this location. Therefore optical amplifiers are more commonly located after the splitter, which means that one amplifier per splitter output is needed instead of one per splitter input. In some distribution applications one set of optical amplifiers is all that is necessary. In other applications with several levels of splitting, one set of optical amplifiers per level of splitting may be needed. Each optical amplifier emits broad-bandwidth noise in addition to the amplified coherent (narrowband) light. If this noise is not reduced through filtering, it is possible for subsequent stages of optical amplification to amplify and eventually be saturated by this broadband light.
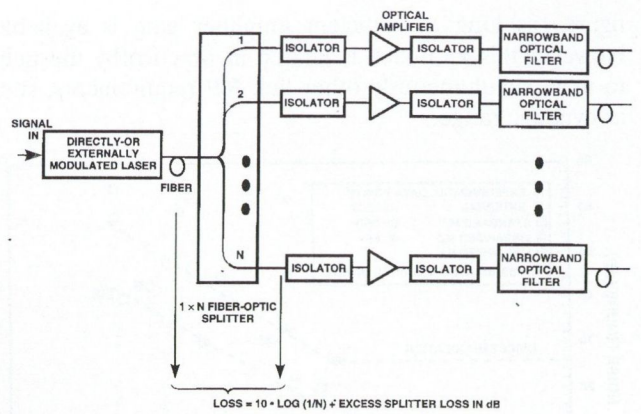

Fig. 3. Distribution link topology showing the use of optical amplifiers and the need in some cases for both optical isolators and filters to prevent oscillations and reduce the wideband output noise

4. RECEIVE LINKS

These links are designed to convey a signal detected by an antenna to a receiver located remotely from the antenna. Examples of receive links include the down-link in a cellular/PCS system and the receive mode in a radar. A typical block diagram of a receive link is shown in Fig. 4.
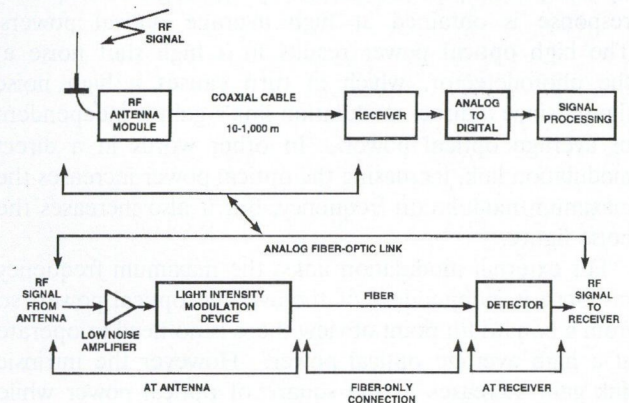

Fig. 4. Receive link topology

Since these links are designed primarily for conveying low level signals from the antenna, low noise figure is one of the primary technical goals for receive links. The data in Fig. 5 summarizes reported experimental link noise figures vs. the 3 dB frequency of the link. Although these noise figures are high, they are not an artifact of casual link design. Rather they are a direct consequence of the high link loss, as shown in Fig. 1. As has been previously shown, the minimum link noise figure is related to the intrinsic gain as $10 \cdot \log(2 + 1/G)$ [8]. At low frequencies, the combination of low link noise figure (as shown in Fig. 5) and high sky noise permit fiber-optic links to be connected to the antenna without the need for any electronic pre-amplification.

As the required link operating frequency increases, the noise figure increases, primarily due to the higher link loss. Consequently virtually all high frequency receive links require a low-noise preamplifier between the antenna and the link input. In principle the high link noise figures can be reduced to nearly the electronic pre-amplifier noise

figures as long as sufficient amplifier gain is available. However this approach is limited in practice by the need to meet simultaneously other link RF requirements, such as dynamic range.
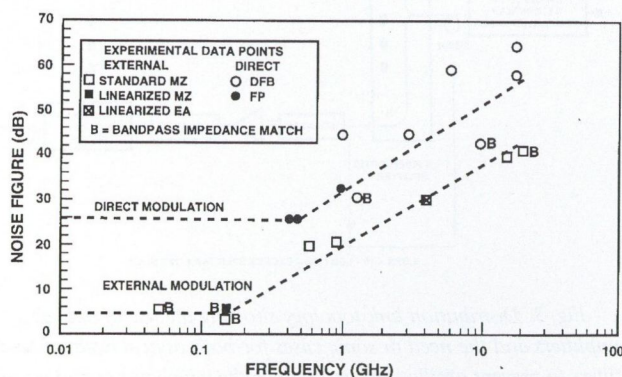

Fig. 5. Noise figure vs. frequency data reported for direct and external modulation links

Techniques for reducing the link noise figure will depend on the method used for impressing the modulation. Recall that in direct modulation links, the laser's relaxation resonance increases as the square-root of the average optical power [9]. Consequently the highest frequency response is obtained at high average optical powers. The high optical power results in a high shot noise at the photodetector, which in turn causes a high noise figure, since a direct modulation link's gain is independent of average optical power. In other words in a direct modulation link, increasing the optical power increases the maximum modulation frequency, but it also increases the noise figure.

For external modulation links, the maximum frequency response is independent of the average optical power, so from a bandwidth point of view there is no need to operate at a high average optical power. However the intrinsic link gain increases as the square of optical power while the shot noise only increases linearly with optical power. Therefore the effect of increasing average optical power actually decreases the noise figure, because the gain is increasing faster than the shot noise. Thus the external modulation noise figure should be easier to reduce, since it does not suffer from the conflicting design constraints that direct modulation does [10].

In addition to noise figure, another important receive link parameter is intermodulation-free dynamic range, IMFDR. One important aspect of many receive links that does simplify the interference problem is that broadband antennas are rare, and those that are broadband achieve a wide bandwidth at a severe tradeoff in sensitivity. Consequently most receive links need only an octave bandwidth or less, which means that second order distortion can be filtered out and that third order distortion dominates the IMFDR. This is an important consideration because all the known broadband linearization techniques — i.e., those that reduce both the second and third order distortion —

invariably increase the noise figure. However third-order-only linearization techniques, which invariably increase the second-order distortion, do not suffer a significant noise figure penalty [11].

All the linearization techniques demonstrated to date have been tested at frequencies below about 1 GHz. Initial attempts to linearize higher frequency links have not realized the amount of increased dynamic range seen at lower frequencies. This effect was first reported by Farwell *et al.* [12] when using their multi-electrode directional coupler modulator to perform linearization. The problem was traced to the need for a higher degree of velocity matching between the RF and optical waves than is required for simply extending the frequency response. Bridges and Schaffner have pointed out [13] that the effects Farwell *et al.* observed are not limited to his device or method, but rather that all linearized modulators will suffer from this effect to a greater or lesser degree.

Like transmit links, receive links often need to operate at high center frequencies. Frequency conversion links have also been investigated for receive links, but in a different form. A block diagram of one version of a frequency conversion link for receive use is shown in Fig. 6. In this figure, the frequency conversion link is basically an external modulation link where the usual CW source has been modulated with the LO signal. One of the early demonstrations of a frequency conversion link was reported by Gopalakrishnan *et al.* [14], who reported at 9 GHz and 16 GHz conversion losses of 19.6 dB and 22.9 dB, respectively, and noise figures of 50.0 dB and 53.3 dB, respectively. This work spurred several workers to investigate ways to implement frequency conversion links without imposing a large noise figure penalty relative to the noise figure of a link without frequency conversion. For example, Sun *et al.* optimized the LO drive waveform and added electrical gain to improve the conversion gain and noise figure [15]. Significant progress has more recently been reported in this area by Helkey *et al.* [5], who achieved an amplifierless conversion gain of 17 dB.
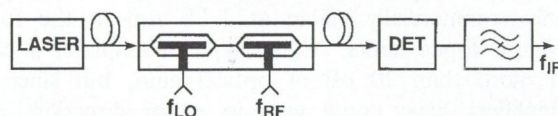

Fig. 6. Block diagram of down-converting fiber-optic link for receive applications

5. ACKNOWLEDGMENTS

REFERENCES

[1] J. Ralston, S. Weisser, K. Eisele, R. Sah, E. Larkins, J. Rosenzweig, J. Fleissner and K. Bender: "Low-bias-current direct modulation up to 33 GHz in InGaAs/GaAs/AlGaAs pseudomorphic MQW ridge-waveguide devices," *IEEE Photon. Technol. Lett.*, Vol. 6, pp. 1076-1079, 1994.

[2] K. Noguchi, H. Miyazawa and O. Mitomi: "75 GHz broadband Ti:LiNbO$_3$ optical modulator with ridge structure," *Electron. Lett.*, Vol. 30, pp. 949-951, 1994.

[3] S. Chou and M. Liu: "Nanoscale Tera-Hertz Metal-Semiconductor-Metal Photodetectors," *IEEE J. Quantum Electron.*, Vol. 28, pp. 2358-2368, 1992.

[4] I. Koffman, P. Herczfeld and A. Daryoush: "High Speed Fiber Optic Links for Short-Haul Microwave Applications," *IEEE Microwave Theory Tech. Symp. Dig.*, Vol. II, pp. 983-986, 1988.

[5] R. Helkey, J. Twichell and C. Cox: "A Down-Conversion Optical Link with RF Gain," *J. Lightwave Technol.*, Vol. 15, pp. 956-961, 1997.

[6] M. O'Mahony: "Semiconductor Laser Optical Amplifiers for Use in Future Fiber Systems," *J. Lightwave Technol.*, Vol. 6, pp. 531-544, 1988.

[7] E. Desurvire: *Erbium-Doped Fiber Amplifiers*, New York, Wiley, 1994.

[8] C. Cox, E. Ackerman and G. Betts: "Relationship Between Gain and Noise Figure of an Optical Analog Link," *IEEE Microwave Theory Tech. Symp. Dig.*, pp. 1551-1554, 1996.

[9] W. Way: "Large signal nonlinear distortion prediction for a single-mode laser diode under microwave intensity modulation," *J. Lightwave Technol.*, Vol. 5, pp. 305-315, 1987.

[10] C. Cox, G. Betts and L. Johnson: "An analytic and experimental comparison of direct and external modulation in analog fiber-optic links," *IEEE Trans. Microwave Theory Techn.*, Vol. 38, pp. 501-509, 1990.

[11] G. Betts: "Linearized modulator for suboctave-bandpass optical analog links," *IEEE Trans. Microwave Theory Techn.*, Vol. 42, pp. 2642-2649, 1994.

[12] M. Farwell, Z. Lin, E. Wooten and W. Chang: "An electro-optic intensity modulator with improved linearity," *IEEE Photon. Technol. Lett.*, Vol. 3, pp. 792- 795, 1991.

[13] W. Bridges and J. Schaffner: "Distortion in linearized electro-optic modulators," *J. Lightwave Technol.*, Vol. 43, pp. 2184-2197, 1995.

[14] G. Gopalakrishnan, R. Moeller, M. Howerton, W. Burns, K. Williams and R. Esman: "A Low-Loss Downconverting Analog Fiber-Optic Link," *IEEE Trans. Microwave Theory Tech.*, Vol. 43, pp. 2318-2323, 1995.

[15] C. Sun, R. Orazi and S. Pappert: "Efficient Microwave Frequency Conversion Using Photonic Link Signal Mixing," *IEEE Photon. Technol. Lett.*, Vol. 8, pp.154-156, 1996.
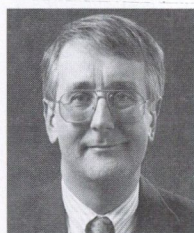
Charles Cox received his BSEE and MSEE degrees in 1970 and 1972 from the University of Pennsylvania and the ScD from MIT in 1979. Since 1979 he has been with MIT Lincoln Laboratory where he has been a technical staff member in the Photovoltaic Systems and the Applied Physics Groups. He is presently a senior staff member in the Applied Photonics section of the Radar Systems Group. For the last 12 years he has pursued, both theoretically and experimentally, the development of electro-optic devices and analog fiber optic links primarily for antenna remoting. Dr. Cox is a senior member of IEEE, a member of Optical Society of America and Sigma Xi.

Edward I. Ackerman received his B.S. degree in electrical engineering from Lafayette College in 1987 and his M.S. and Ph.D. degrees in electrical engineering from Drexel University in 1989 and 1994, respectively. From 1989 through 1994 he was employed as a microwave photonics engineer at Martin Marietta's Electronics Laboratory in Syracuse, New York. Currently he is a member of the Technical Staff at MIT Lincoln Laboratory in Lexington, Massachusetts, where he develops high-performance analog photonic links for microwave communications and antenna remoting applications.
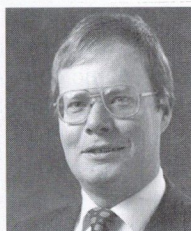
Roger Helkey received the B.S. degree in engineering with honors from the California Institute of Technology in 1982, and the M.S. degree and Ph.D. degree in electrical engineering from the University of California, Santa Barbara, in 1993. His graduate work was on modelocked semiconductor lasers. From 1993 to 1995, he was a researcher at the University of Tokyo and at Advanced Telecommunications Research in Japan, studying microcavity effects and nonlinear optical switching. From 1982 to 1984, he was a design engineer at Trimble Navigation where he was responsible for the design of digital and analog circuits in the development of a Global Positioning System (GPS) receiver. From 1984 to 1986, he was a Member of the Technical Staff at Watkins-Johnson, where he was responsible for microwave component and subsystem design. He is currently a staff member at MIT Lincoln Laboratory where he is working on high dynamic range analog optical links. He is the coauthor of a book chapter and holds several patents.
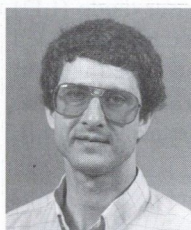
Gary E. Betts received the B. S. degree in physics from Haverford College, Haverford, PA in 1976, the M.S. degree in physics and the Ph.D. degree in applied physics from the University of California at San Diego in 1980 and 1985, respectively. His thesis work dealt with electro-optic modulators in lithium niobate. From 1976 to 1978 he worked in integrated optics, primarily on the design of geodesic lenses, at the Westinghouse Electric Corporation, Baltimore, MD. Since 1985 he has been a staff member at the MIT Lincoln Laboratory, Lexington, MA working primarily on lithium niobate integrated-optical modulators and analog fiber optic links. His work at MIT has included microwave-frequency modulators, low frequency modulators with very high sensitivity, linearized modulators, investigation of optical damage and other drift phenomena in lithium niobate, and most recently, work on high powered semiconductor optical amplifiers. He is a member of the Optical Society of America and the IEEE Lasers and Electro-Optics Society.

FREQUENCY CONVERSION METHODS
BY INTERFEROMETER AND PHOTODIODE
IN MICROWAVE OPTICAL LINKS

A. HILT, G. MAURY, B. CABON, A. VILCOT and T. BERCELI

LEMO-ENSERG-INPG, INSTITUT NATIONAL POLYTECHNIQUE DE GRENOBLE
23 RUE DES MARTYRS, BP 257, F-38016 GRENOBLE, CEDEX 1, FRANCE

BME-MHT, TECHNICAL UNIVERSITY OF BUDAPEST, DEPARTMENT OF MICROWAVE TELECOMMUNICATIONS
H-1111 BUDAPEST, GOLDMANN GYÖRGY TÉR 3., HUNGARY
TKI RT, INNOVATION COMPANY FOR TELECOMMUNICATIONS
H-1142 BUDAPEST, UNGVÁR UTCA 64-66., HUNGARY

Recently fiber optic links have been investigated by several authors for the transmission and distribution of microwave and millimeter-wave signals [1], [2]. For further signal processing, frequency conversion is necessary in several applications, e.g. wireless distribution of optically received signals [3]. Efficient mixing methods are required for this purpose to simplify the complexity of the system.

1. INTRODUCTION

The traditional solution employs electronic mixers for the frequency conversion of detected optical signals that are modulated by RF signals. However, adding or benefiting of nonlinearities in the optical link, frequency conversion can be done eliminating electronic mixers. Two alternative methods for conversion are presented and compared in this paper. In the first case, the optical link is completed by a passive optical component, an unbalanced Mach–Zehnder interferometer (UMZ) and mixing is performed on RF modulated optical signals. The optical intensity contains mixing products and it is detected by a photodiode (PD) at the end of the link. In the second case, the mixing is done by a high speed pin PD itself, having electronic and optical excitation simultaneously.

2. MIXING WITH UMZ/PD

1.1. Principle

The optical system used for microwave mixing is shown in Fig. 1. A distributed feedback (DFB) laser diode (LD) is directly modulated by two microwave frequencies added by an RF combiner. The optical power is coupled into an optical fiber and injected to an UMZ interferometer. The PD converts the optical intensity into electrical current [4].
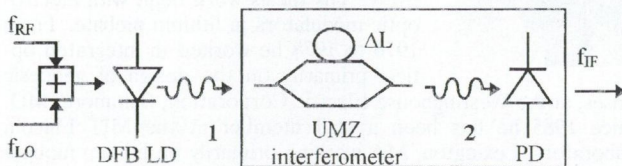

Fig 1. Optical system used for microwave mixing

The basic principle is the nonlinear (sinusoidal) intensity response of the UMZ interferometer/PD combination as a function of the optical frequency [5]. Direct current

modulation generates frequency modulation (FM) which is then converted to AM using the UMZ interferometer working in the coherent regime. The PD detects the optical intensity which is a quadratic function of optical amplitude, so frequency mixing is obtained. This technique is analogous to the one using an interferometric modulator biased for maximum or minimum transmission. In both cases, the nonlinearity of the light intensity response at modulation frequencies is used: in the external modulator the path length ΔL of the interferometer rather than the frequency of the light is modulated. Here, the path length ΔL of the interferometer remains constant. Therefore, the component can be made of passive and low-loss material such as optical fiber or optical integrated waveguide which can minimize the total conversion loss, to a much lower value than the external active modulator.

The LD driving current is directly modulated by two microwave frequencies f_1, (e.g. f_{LO} corresponding to the local oscillator signal) and f_2 (in this case, f_{RF}). We consider here that the PD is operating under a linear regime and, as mixing is mainly issued from the FM, we consider the case in which AM is negligible. So the complex expression of the electrical field of the optical signal may be written as:

$$E(t) =$$
$$E_0 \exp\{j[2\pi\nu_0\tau + \beta_1 \sin(\omega_1 t) + \beta_2 (\sin(\omega_2 t)]\} \quad (1)$$

where ν_0 is the optical frequency, β_i is the FM index and ω_i is the angular modulation frequency.

At the output of the interferometer, with delay time τ between the two arms and assuming no propagation loss, the intensity is given by:

$$I(t) = \frac{E_0^2}{2} \{1 + V(\tau) \cos 2 [\pi\nu_0\tau +$$
$$\beta_1 \sin\left(\omega_1 \frac{\tau}{2}\right) \cos\left(\omega_1 \left(t + \frac{\tau}{2}\right)\right) + \quad (2)$$
$$\beta_2 \sin\left(\omega_2 \frac{\tau}{2}\right) \cos\left(\omega_2 \left(t + \frac{\tau}{2}\right)\right)]\} .$$

$V(\tau)$ reflects the loss of coherence between the electric field in the two arms of the MZ interferometer. In the coherent working regime $V(\tau) = 1$ and in the incoherent regime $V(\tau) = 0$. As it can be seen, in the coherent working regime, the optical intensity contains

harmonics and intermodulation products, including the mixing products at frequencies $f_{IF} = f_1 \pm f_2$. When the interferometer is balanced on a "bright" or a "dark" fringe i.e.: $\cos(2\pi\nu_0\tau) = \pm 1$, the resulting intensity is generated at harmonics and intermodulation products of even order (of the form $nf_1 \pm mf_2$ with $n + m \in 2Z$) and, in particular, at the mixing frequency f_{IF}. When the interferometer is balanced on a "gray" fringe i.e. $\sin(2\pi\nu_0\tau) = \pm 1$, the intensity is generated at harmonics and intermodulation products of odd order. As a consequence, the passive MZ interferometer operating at minimum or maximum transmission acts as a mixer at frequency f_{IF}. Thus, $\cos(2\pi\nu_0\tau) = \pm 1$ is the best condition to obtain the maximum power at frequency f_{IF}, that we call condition 1.

To be optimized, the output spectrum of the optical intensity must exhibit the maximum power of the mixing frequency. Condition 2 is fulfilled when:

$$f_1 = (2k+1)\frac{\text{FSR}}{2} \quad \text{and} \quad f_2 = (2k'+1)\frac{\text{FSR}}{2}, \quad (3)$$

where k and $k' \in N$, $\text{FSR} = 1/\tau = c/(n_{\text{eff}}\Delta L)$ is the Free Spectral Range of the interferometer. Therefore, the difference of input frequencies must be as close as possible to a multiple of FSR. For given input microwave frequencies, the path length difference ΔL must be chosen to match these conditions.

The response at the PD output depends on the input microwave frequencies. With an UMZ interferometer, the response is periodic with the input frequencies: it means that the device works optimally not for all frequencies but for particular frequencies in any frequency range. Within one period, the 3 dB bandwidth approximates FSR/2.

Finally, the power of the mixing frequency delivered into a 50 Ω load at the PD output can be easily calculated:

$$P = \frac{R_0}{2}R^2 E_0^4 J_1^2(2\beta_{\text{RF}}) J_1^2(2\beta_{\text{LO}}) \quad (4)$$

where $R_0 = 50\ \Omega$, R is the PD responsivity and J_1 is the first order Bessel function. In the best case, P_{LO} is chosen such as $J_1^2(2\beta_{\text{LO}})$ is maximum and equal to 0.58^2. Generally, P_{RF} is low so as β_{RF}.

1.2. Simulation Results

In practice, AM is not always negligible. By Fourier transform, we can calculate the power of the different frequency components in the PD current in the general case, as a function of different parameters such as operating frequencies, input power levels, etc.

We have simulated a LD with linewidth enhancement factor $\alpha = 5$, threshold current $I_{\text{th}} = 15$ mA, biased at $I_0 = 30$ mA. The optical power coupled in the optical fiber is assumed to be 1 mW. The effective index of the fiber is $n_{\text{eff}} = 1.46$. The mixing product $f_{IF} = f_2 - f_1$ is chosen to be 1 GHz. The path length difference ΔL is calculated making the FSR and the mixing frequency equal in order to fulfill Condition 2:

$$\Delta L = \frac{c}{n_{\text{eff}}\text{FSR}} = \frac{c}{n_{\text{eff}}(f_2 - f_1)} = 0.205\ \text{m}. \quad (5)$$

First, the conversion was calculated, as the difference between the power of the mixing component and the RF

input power, as a function of P_{LO}, with a very low P_{RF} of -20 dBm, for an example of optimized frequencies ($f_1 = 10.5$ GHz and $f_2 = 11.5$ GHz). It is also assumed that the interferometer works in the coherent regime and at maximum transmission. The results are plotted in Fig. 2a. As in the simplified case with AM neglected, here the calculations exhibit also an optimal P_{LO} for which the loss is minimum. The variation of the conversion with P_{RF} (see Fig. 2b) when $P_{\text{LO}} = -7.1$ dBm shows a flat response at low RF values, and a significant increase of loss is observed for $P_{\text{RF}} > -8$ dBm.
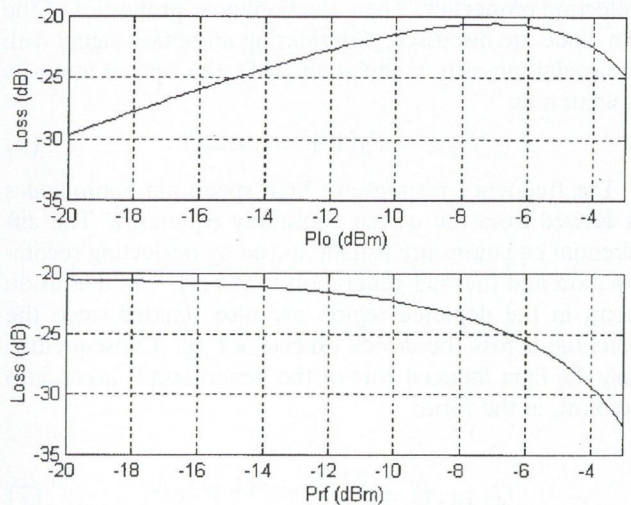

Fig. 2. Variations of the conversion with P_{LO} (a) and with P_{RF} (b)

Then, the power of the different frequency components were simulated at the PD output as function of f_1 varying in a band equal to FSR, with the optimal $P_{\text{LO}} = -7.1$ dBm and $P_{\text{RF}} = -20$ dBm. Fig. 3 corresponds to the case of maximum transmission of the interferometer. It is confirmed that the maximum power of f_{IF} is obtained at $f_1 = 10.5$ GHz. For this frequency, the fundamentals f_1 and f_2 are rejected. More generally, it can be noticed that the mixing frequency can be the sum or the difference of the input frequencies and that these two cases exhibit quite the same power in Fig. 3.
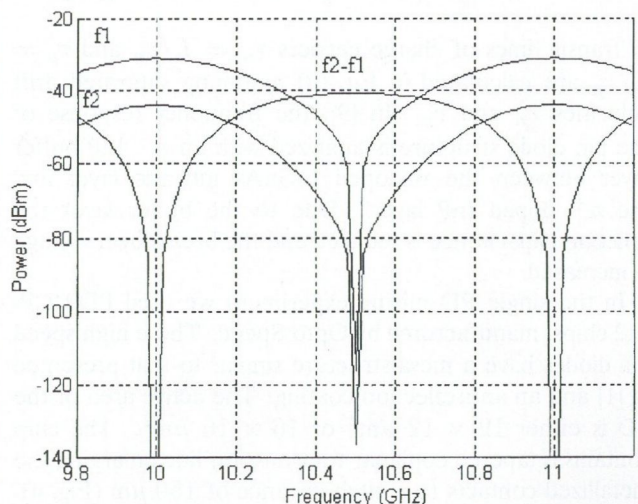

Fig. 3. Power of the frequency components after detection

In conclusion, simulations confirm the possibility of realizing the mixing function with an UMZ interferometer operating at maximum or minimum of transmission. Conversion can be very good and gain is obtained instead of loss if the LD emits large optical power and has an important linewidth enhancement factor ($\alpha > 5$).

2. MIXING BY PHOTODIODES

2.1. Photodiode Characterization

First the PD is characterized by its DC and high speed detection properties. Then, the nonlinear properties of the pin diode are discussed. Considering an optical signal with sinusoidal intensity modulation (IM), the optical intensity is written as:

$$P_{\text{opt}} = P_0(1 + m \cos \omega t) . \tag{6}$$

The frequency response of high speed pin photodiodes is derived from the carrier continuity equations. The differential equations are usually solved by neglecting recombination and thermal generation terms [7]−[9]. Diffusion terms in the depleted region are also omitted since the potential across the device exceeds kT/q. Consequently, only the light induced part of the generation is taken into account, in the form:

$$G_L(x,t) = \frac{\alpha \eta P_0}{h\nu} e^{-\alpha(L-x)} e^{j\omega t} \tag{7}$$

where L is the thickness of the intrinsic layer, α is the absorption coefficient, η is the quantum efficiency, $e^{j\omega t}$ is due to the IM given in Eq. (6) and an illumination from the n side is supposed. Finally, the frequency response $H(\omega)$ is given as the alternating PD current normalized to the DC term [7], [9]:

$$H(\omega) = \frac{i(\omega)}{I(0)} = \frac{1}{1 - e^{-\alpha L}} \left[\frac{e^{j\omega \tau_n - \alpha L} - 1}{j\omega \tau_n - \alpha L} - \right. \tag{8}$$
$$\left. e^{-\alpha L} \frac{e^{j\omega \tau_n} - 1}{j\omega \tau_n} + \frac{e^{-\alpha L} - e^{j\omega \tau_p}}{j\omega \tau_p + \alpha L} + \frac{e^{j\omega \tau_p} - 1}{j\omega \tau_p} \right] .$$

Transit times of charge carriers $\tau_n = L/v_n$ and $\tau_p = L/v_p$ are calculated in Eq. (8) assuming saturated drift velocities v_n and v_p. In [9], the frequency response of the pin diode structure is analyzed with an n^- InP buffer layer between the undoped InGaAs intrinsic layer and the n^+ doped InP layer. Due to the buffer layer the junction capacitance is reduced and the breakdown voltage is increased.

In the single PD mixing experiment we used PD94CP-S12 chips, manufactured by Opto Speed. These high speed pin diodes have a mesa structure similar to that presented in [1] and an antireflection coating. The active area of the PD is either $12 \times 12 \ \mu m^2$ or $16 \times 16 \ \mu m^2$. The chip contains a tapered coplanar transmission line enlarging the metallized contacts to a pitch distance of $150 \ \mu m$ (Fig. 4). The coplanar structure allows direct probe measurements.

Impulse response measurements using very short pulse transients have been performed by the manufacturer. Due

to the small active area, rise and fall times shorter than 18 ps have been obtained, corresponding to a cut off frequency higher than 50 GHz.
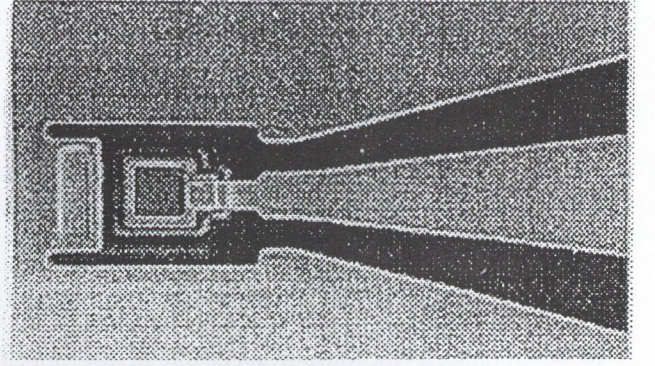

Fig. 4. Opto Speed pin PD chip with tapered coplanar line

We characterized the PD by frequency domain measurements. The PD responsivity R (optical-to-electrical (O/E) conversion) is frequency dependent due to Eq. (8) and is given in dB(A/W) units defined as:

$$R(\omega)[dB(A/W)] = 20 \log \frac{R(\omega)[A/W]}{1[A/W]} . \tag{9}$$

Applying higher reverse bias voltage, which results higher electric field across the depleted region, the flatness of the response is improved due to the significant reduction of charge carrier transit times (Fig. 5).
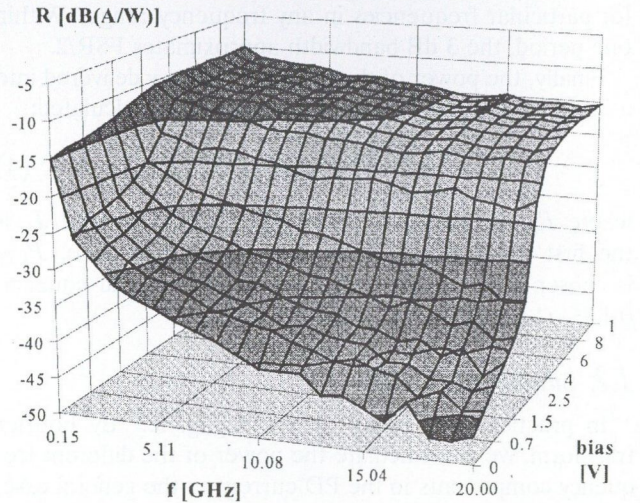

Fig. 5. Responsivity of $12 \times 12 \ \mu m^2$ photodiode $P_{\text{opt}} = 323 \ \mu W$, $f = 0.45 \ GHz \ldots 20 \ GHz$

The response of Fig. 5 was measured directly by a Cascade Microtech ACP40 air-coplanar wafer probe connected to a HP 8510B Vector Network Analyzer (VNA). The VNA was extended by a HP 83420A LightWave Test Set (LWTS) including a DFB laser source emitting at $\lambda = 1.3 \ \mu m$. The optical signal was intensity modulated up to 20 GHz by the external MZ interferometer modulator. The optical modulation depth (OMD) was m=25 %. In this arrangement responsivity and electrical reflection of the PD have been measured as a function of modulation frequency and light intensity.

2.2. Principle of Optical-Microwave Mixing

The optical-microwave mixing employing high speed PDs has been analyzed based on the DC characteristics [6]. The DC characteristics measured at different optical intensities illuminating the device are shown in Fig. 6. To achieve good responsivity the PD is used in its saturation regime so a strong reverse bias voltage is applied (Fig. 5). The reverse bias is usually several Volts, consequently the device is rather linear at low light injection levels [10], [11].
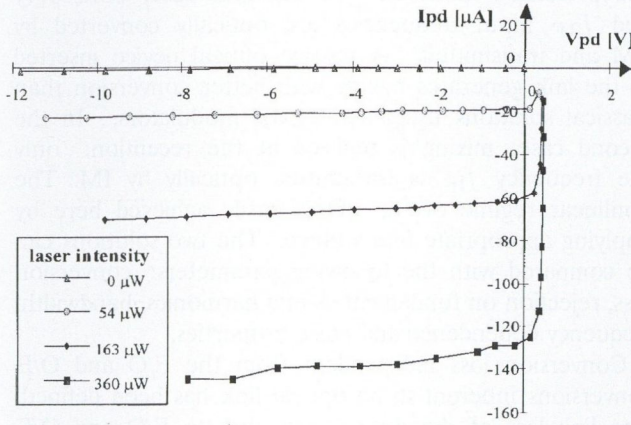
Fig. 6. Current-voltage characteristics of PD illuminated by different optical intensities

Simultaneously injecting a microwave signal at the electrical port and a modulated optical signal at the optical port of the PD, mixing of the two signals occurs. However, the optimal bias points for efficient mixing and for efficient detection are significantly different. The mixing process is explained as a result of the nonlinearity of the PD current-voltage relationship. Due to the fact that the current-voltage characteristics exhibit the maximum non-linearity in the vicinity of 0 V, it is the optimal operation point for efficient mixing. Thus the mixing product has maximum power around this voltage [2], [6], [12].

Detection the IM signal of Eq. (6) is written as:

$$P_{IF} = A_{DET} \cos \omega_{IF} t \,. \tag{10}$$

Due to the nonlinearity, several mixing products of both the microwave driving signal at f_{LO} and the photo induced signal at f_{IF} are generated. Using a microwave LO signal $f_{LO} > f_{IF}$, the detected optical signal is upconverted and written in the form:

$$P_{MIX}(t) = A_{LO} \cos \omega_{LO} t + A_{IF} \cos \omega_{IF} t +$$

$$A_2 \cos(\omega_{LO} \pm \omega_{IF})t + A_3 \cos(2\omega_{LO} \pm \omega_{IF})t + \tag{11}$$

$$A_4 \cos(\omega_{LO} \pm 2\omega_{IF})t + \dots$$

Since the LO signal is partly reflected at the illuminated PD, frequency f_{LO} is also present in $P_{MIX}(t)$ at the output.

3. EXPERIMENTAL RESULTS

3.1. Experimental Results with UMZ/PD

Measurements were made with a $\lambda = 1.3$ μm DFB LD, with $I_{th} = 13$ mA and a maximum oscillation frequency of 2.5 GHz. The DC bias current was 22 mA and the

optical power coupled in the optical fiber was 420 μW. Reflections on the fiber generate optical feedback in the LD and thus decrease its coherence length: to operate in the coherent regime as wanted, ΔL must not exceed 30 cm. For this reason, the UMZ was realized using only two 3 dB fiber directional couplers with $\Delta L = 1.6$ cm which corresponds to FSR = 13 GHz. The New Focus rapid PD used has an ultra wide bandwidth of 45 GHz and a responsivity of $R = 0.356$ mA/mW.

Using a fiber UMZ interferometer, two problems are arising. First the instability of polarization state of the optical field at the output of the two interferometer arms. The second is the instability of the relative optical phase shift between the two arms, which is very sensitive to ambient variations. For the first reason, the power at the UMZ interferometer output is unstable. Due to the other reason, during the experiments the operating regime varied continuously between minimum and maximum transmission including the quadrature.

The LO frequency was $f_{LO} = 1.9$ GHz, with a power of -4 dBm. Frequency f_{RF} was swept from 2 to 2.5 GHz and had a power of -18 dBm. Fig. 7 shows the measured power spectrum of the intensity detected by the PD. We can compare the two signals, one present at the LD output (point 1 in Fig. 1) and the other present at the interferometer output (point 2 in Fig. 1).
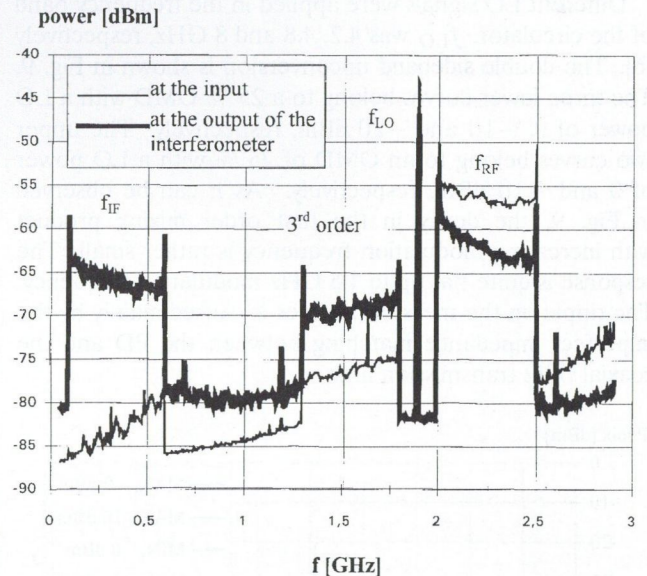

Fig. 7. Power spectra of detected signals

In Fig. 7 the lower sideband of the mixing product, $f_{LO} - f_{RF}$, as well as the third order intermodulation product was significantly increased by inserting the interferometer. But the input frequencies f_{LO} and f_{RF} are not rejected. In fact, to obtain an optimal rejection of the fundamentals, the condition $\cos(2\pi\nu_0\tau) = \pm 1$ should be fulfilled first. Unfortunately it was not the case under unstable conditions of operation of the UMZ. Secondly, the closer f_1 would be to FSR/2 = 6.5 GHz, the larger would be the rejection. The LD modulation bandwidth was the main limiting factor here.

3.2. Experimental Results with PD

Investigating the frequency conversion, a PD bonded with gold wires onto an SMA connector was illuminated by the DFB LD. The LO signal was fed to the PD through a wideband circulator (4.5−9.5 GHz) separating the LO input and the RF output as shown in Fig. 8. In the experiment reported in [12], the upconverted signal was amplified by an amplifier stage following the PD. In our experiments microwave amplifier was not used to avoid further nonlinearities. The upconverted mixing product has been measured by a spectrum analyzer.
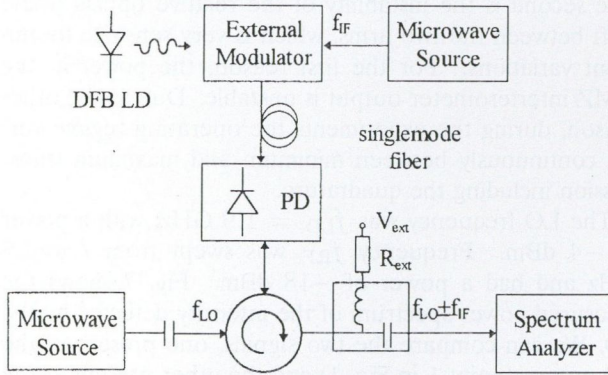
Fig. 8. Experimental setup for PD optical-microwave upconversion

Different LO signals were applied in the frequency band of the circulator, f_{LO} was 4.2, 4.8 and 8 GHz, respectively [6]. The double sideband upconversion is shown in Fig. 9. The three lower curves belong to a 25 % OMD with a LO power of 0, −10 and −20 dBm, respectively. The upper two curves belong to an OMD of 75 % with a LO power of 0 and −10 dBm, respectively. As it can be observed in Fig. 9, the decay in the first order mixing product with increasing modulation frequency is rather small. The response is quite flat up to 1.5 GHz modulation frequency. The ripple on the measured curves is caused mainly by the imperfect impedance matching between the PD and the coaxial 50Ω transmission lines.
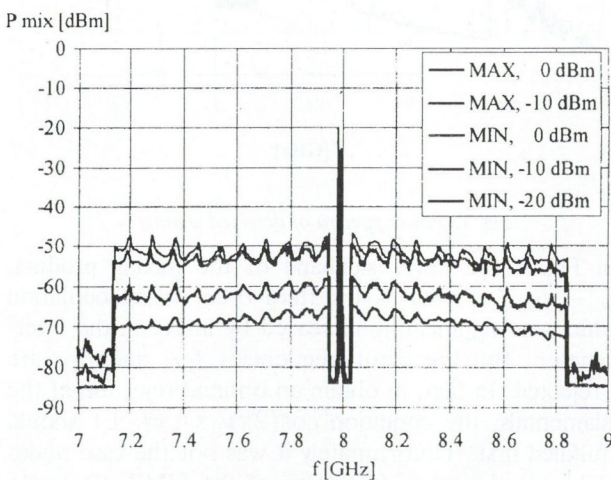

Fig. 9. Upconverted signal by PD mixing, $f_{LO} = 8$ GHz, $P_{LO} = 0, -10, -20$ dBm, $m = 25$ % (MIN) and 75 % (MAX), $f_{mod} = 45...850$ MHz, $P_{opt\ avg} = 290\ \mu W$

At low levels, the power of the mixing product is proportional to the OMD and LO power ($P_{LO} < -5$ dBm). At higher levels a saturation effect is observed ($P_{LO} \cong 0$ dBm). However, the frequency behaviour in Fig. 9 is depending neither on varying the OMD nor the LO power.

4. COMPARISON OF THE TWO METHODS

The principle of frequency conversion is different in the presented methods. In the first case, both f_{LO} and f_{RF} input frequencies are optically converted by FM and transmitted. A passive optical device inserted in the link generates mixing with better conversion than classical solutions using active MZ modulators. In the second case, mixing is realized at the reception: only the frequency f_{IF} is transmitted optically by IM. The nonlinear regime of the PD is easily achieved here by applying appropriate bias voltage. The two solutions can be compared with the following parameters: conversion loss, rejection on fundamentals and harmonics, bandwidth, frequency dependence and noise properties.

Conversion loss independent from the E/O and O/E conversions inherent in an optical link has been defined. The link loss of the optical path due to E/O and O/E conversions (≈ 50 dB in both cases) can be treated separately. In the first case, the conversion loss is the difference between the power of the IF component with the configuration including the UMZ in the optical link and the power at frequency f_{RF} detected by the PD without inserting th UMZ interferometer. In the second case, the conversion loss is defined as the difference of the power detected at f_{IF} using the PD in its linear regime and the signal levels at $f_{LO} \pm f_{IF}$ frequencies upconverted by the PD nonlinearity.

The measured conversion loss varies typically between −10 and 0 dB. However, the conversion loss is a function of several parameters such as the optical intensity of the LD, the OMD, the PD bias, the modulation frequency, or the P_{LO}. Theoretically, conversion gain is also possible in both cases.

By the proper selection of ΔL, the fundamental frequencies f_{LO} and f_{RF} can be rejected by UMZ. In the single PD mixing, the fundamental frequencies are not rejected (Fig. 9). However, in our experiments, f_{IF} was filtered by the circulator passband. In [12], f_{LO} is suppressed by electronic filter. In [2], balanced mixing has been realized by two PDs.

Concerning the bandwidth, in the first case, the response is periodic (Fig. 3). The period FSR is inversely proportional to ΔL. So the bandwidth is increased by reducing ΔL. The response is strongly dependent on the input frequencies f_{LO} and f_{RF}. However, in some applications, it is advantageous since the UMZ device acts as a microwave filter too [13]. By PD mixing, the bandwidth and the frequency dependence are the result of a compromise. The optimal bias points for detection and mixing are different. But applying high speed PD, the frequency dependence of the response is relatively small in a large bandwidth proposing an advantage in applications like reception of SCM optical signals.

5. CONCLUSION

Optical-microwave mixing was investigated for both up and down conversion using two different approaches, one with an UMZ interferometer / PD combination and the other with a high speed pin PD. Both solutions permit to mix microwave frequencies in optical links, which is a new approach compared to the traditional solutions using electronic mixers. Efficient frequency conversion was measured in both cases. The frequency dependence of the converted signals has been investigated by simulations and measurements.

REFERENCES

[1] F. Deborgies, E. Goutain, Y. Combemale, J. C. Renaud and D. Rondi: "New Concepts for Millimeter Wave Optical Links", *Proc. of the 26th EuMC*, Prague, Czech Republic, Vol. 2, pp. 1001-1003, Sept. 1996.

[2] H. Kamitsuna and H. Ogawa: "Fiber Optic Microwave Links Using Balanced/Image Canceling Photodiode Mixing", *IECIE Trans. Electron.*, Vol. E76-C, No. 2, pp. 264-269. Feb. 1993.

[3] D. M. Polifko and H. Ogawa: "Fiber-Optic Link Architectural Comparison for Millimeter Wave Transmission", *SPIE Proc. series, Optical Technology for Microwave Applications VI*, pp. 228-239, Vol. 1703, Orlando, Florida, 20-23 April 1992.

[4] G. Maury and B. Cabon: "Microwave optical mixing with a frequency modulated laser and an unbalanced Mach–Zehnder interferometer", *CLEO / Europe-EQEC'96*, Hamburg, Germany, 1996.

[5] E. Eichen: "Interferometric generation of high power, microwave frequency, optical harmonics", *Applied Physics Letters*, 51, pp. 398-400, 10 Aug. 1987.

[6] T. Berceli, B. Cabon, A. Hilt and G. Járó: "Improved Optical-Microwave Mixing Process Utilizing High Speed Photo- diodes", *Proc. of the 26th EuMC*, pp. 125-129, Prague, Czech Republic, Sept. 1996.

[7] J. E. Bowers, C. A. Burrus and R. J. McCoy: "InGaAs PIN Photodetectors with Modulation Response to Millimeter Wavelengths", *Electronics Letters*, Vol. 21, No. 18, pp. 812-814, 29 Aug. 1985.

[8] R. Sabella and S. Merli: "Analysis of InGaAs P-I-N Photodiode Frequency Response", *IEEE Journal of Quantum Electronics*, Vol. 29, No. 3, pp. 906-916, March 1993.

[9] M. Makiuchi and M. Yano: "Flip-Chip Planar GaInAs/InP p-i-n Photodiodes Analysis of Frequency Response", *Journal of Lightwave Technology*, Vol. 14, No. 1, Jan. 1996.

[10] K. J. Williams, R. D. Esman and M. Dagenais: "Nonlinearities in p-i-n Microwave Photodetectors", *Journal of Lightwave Technology*, Vol. 14, No. 1, pp. 84-96, Jan. 1996.

[11] M. Dentain, B. De Cremoux: "Numerical Simulation of the Nonlinear Response of a p-i-n Photodiode Under High Illumination", *Journal of Lightwave Technology*, Vol. 8, No. 8, Aug, 1990.

[12] Q. Z. Liu, R. Davies and R. I. MacDonald: "Experimental Investigation of Fiber Optic Microwave Link with Monolithic Integrated Optoelectronic Mixing Receiver", *IEEE Trans. on Microwave Theory and Techniques*, Vol. 43, No. 9, pp. 2357-2360, Sept. 1995.

[13] A. Ho-Quoc and S. Tedjini: "Experimental Investigation on the Optical Unbalanced Mach–Zehnder Interferometers as Microwave Filters", *IEEE Microwave and Guided Wave Letters*, Vol. 4, No. 6, June 1994.

Attila Hilt graduated in electrical engineering at the Technical University of Budapest, BME in 1990. He has been with TKI, the Research Institute for Telecommunications, Budapest, since 1989, where he was involved in the development of microwave and millimeter-wave circuits and systems. Presently he is a Ph.D. student at LEMO, ENSERG, INPG, in France and at the Microwave Telecommunications Department of BME. The subject of his thesis includes microwave-optical interactions and optical control of microwave circuits and semiconductors.

Béatrice Cabon received the Ph.D. degree in microelectronics in 1986. She worked from 1986 to 1989 at CNET, the National Center of Telecommunications, in the field of CAD and modeling of microelectronic components. Since 1989, she has been an Associate Professor at INPG and trains engineering students in electronics and microwave engineering. She joined the LEMO (Laboratory of Electromagnetism, Microwaves, and Optoelectronics) in 1989. Her research interests have been the modeling of propagation characteristics of various passive superconductive circuits. She is presently bead of a research group of optics/microwave interactions, and she is involved in the optical processing of microwave signals.

Ghislaine Maury obtained the grade of engineer in telecommunications from 'École Nationale Superieure des Télécommunications of Paris and the 'Diplôme d'Études Approfondies' in electronics in 1995. She is presently a Ph.D. student at 'Laboratoire d'Électromagnétisme, Micro-ondes et Optoélectronique' (LEMO), ENSERG, 'Institut National Polytechnique de Grenoble' (INPG), in France. The subject of her thesis incorporates optical-microwave signal processing.

Anna Vilcot obtained the grade of engineer in electronics from INPG, France, and the 'Diplôme d'Études Approfondies' in Optics, Optoelectronics and Microwaves from INPG in 1989. There, she submitted her Ph.D. thesis entitled "Modeling in Microwaves of Planar Transmission Lines and Discontinuities", 1992, which had been prepared at the LEMO. Since 1993, she has been an associate professor at INPG, where she teaches courses on electromagnetism and microwaves. She is doing her research in the Optics/Microwaves team, on the optical control of microwave circuits.

Tibor Berceli for a photograph and biography, see p. 1.

NOISE PROPERTIES OF OPTICAL RECEIVERS USING DISTRIBUTED AMPLIFICATION

G. JÁRÓ,   A. HILT,   A. ZÓLOMY   and   T. BERCELI

BME-MHT, TECHNICAL UNIVERSITY OF BUDAPEST, DEPARTMENT OF MICROWAVE TELECOMMUNICATIONS
H-1111 BUDAPEST, GOLDMANN GYÖRGY TÉR 3., HUNGARY

TKI RT., INNOVATION COMPANY FOR TELECOMMUNICATIONS
H-1142 BUDAPEST, UNGVÁR UTCA 64-66., HUNGARY

In wideband optical communications the bandwidth and the noise of optical receivers are crucial problems. The application of a distributed amplifier instead of a transimpedance amplifier in an optical receiver has the advantage of high speed and low noise [1], [2]. The characteristics of an optical receiver are not only determined by the parameters of the photodiode (PD) and the distributed amplifier driven by the diode, but they are also greatly influenced by the matching circuit [3]. In this paper the gain and the input equivalent noise current of the amplifier are compared in different matching configurations. One of the matching circuits has been experimentally verified as well.

1. INTRODUCTION

There is an increasing demand for high speed digital or analog microwave optical communication links (Fig. 1). For this purpose optical receivers with extreme bandwidth and low noise are required [4].
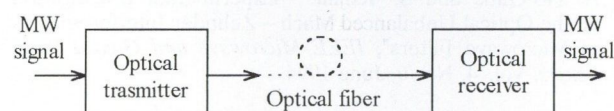
Fig. 1. Microwave fiber optic link

The bandwidth of optical receivers is limited either by the physical parameters of the photodiode or by the external electrical circuit [5]. The electrical circuit contains a microwave amplifier and a matching circuit (Fig. 2).
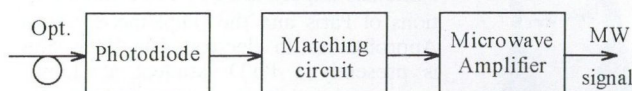

Fig. 2. High speed optical receiver

Distributed amplification is a very attractive solution in ultra-wideband signal processing [6]. In this paper the effect of the matching circuit between the photodiode and the distributed amplifier is investigated.

2. FOUR-STAGE DISTRIBUTED AMPLIFIER MODEL

A four-stage distributed amplifier (DA) matched to 50 Ω input and output impedances is modeled with lumped elements. Fig. 3 shows the schematic of the amplifier.

The field effect transistors in the amplifier are represented by gate and drain capacitances, and voltage controlled current sources as shown in Fig. 4.
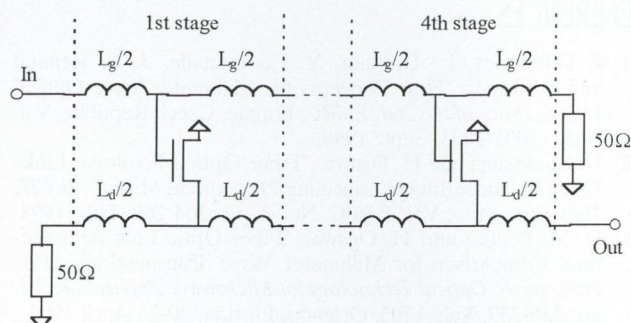

Fig. 3. Schematic of a four-stage distributed amplifier with lumped elements
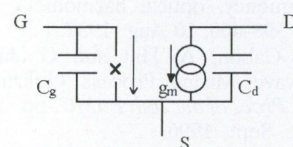

Fig. 4. Equivalent circuit model of the transistor

Inserting the transistor model into the amplifier leads to an LC transmission line structure, as shown in Fig. 5.
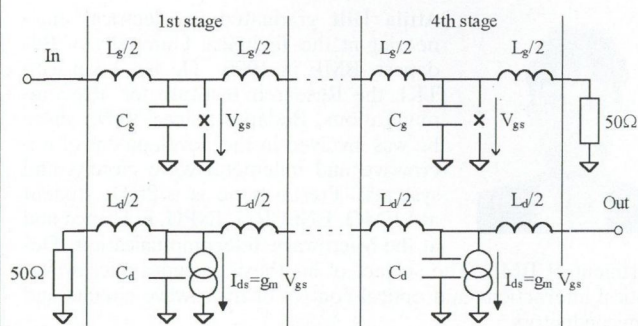

Fig. 5. Lumped model of the four-stage DA

For typical FET element values, the gain of the amplifier is $S_{21} = 14$ dB, while the input and the output reflections (S_{11} and S_{22}) are smaller than -20 dB in the frequency range of $0-15$ GHz. Assuming $C_g = 0.2$ pF, $C_d = 0.1$ pF and $g_m = 50$ mS, the value of L_g and L_d are 449 pH and 322 pH, respectively. Fig. 6 shows the equivalent circuit model (in this case up to 15 GHz) of the four-stage distributed amplifier of Fig. 5.
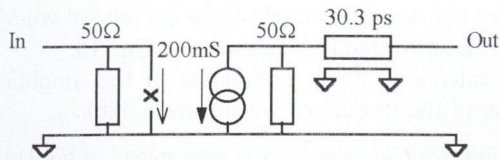
Fig. 6. Equivalent circuit model of the distributed amplifier

This general distributed amplifier model which consists of an ideal amplifier and a delay line has been used to compare the different photodiode and amplifier interconnections based on computer simulations [7].

3. GAIN CHARACTERIZATION

To connect the photodiode and the DA, some possible matching methods are indicated in Fig. 7. For a reference transimpedance in the case of Fig. 7a, the amplifier is driven by a combination of a current source and a 50 Ω resistor. The receiver gain is described by the transimpedance:

$$Z_{\mathrm{tr}} = \frac{V_{\mathrm{out}}}{I_{\mathrm{in}}}, \ Z_{\mathrm{tr}} \ [\mathrm{dB\Omega}] = 20 \log \frac{|Z_{\mathrm{tr}}|}{1\Omega} \ .$$

The photodiode is modeled by a current source and a parallel 0.5 pF capacitance (in all cases the PD is substituted with these elements). The transimpedance gain of the receiver has been calculated for each case as a function of frequency and it is presented in Fig. 8. The circuit parameters were choosen for maximally flat gain (except Case e where the matching circuit elements were choosen for maximally flat input impedance).

The simplest connection between the photodiode and the amplifier is the direct connection as it is shown in Fig. 7b. The gain at low frequency is 6 dB higher than in the resistive generator case but at high frequency it has about the same value, due to the monotonous descent of the transimpedance.
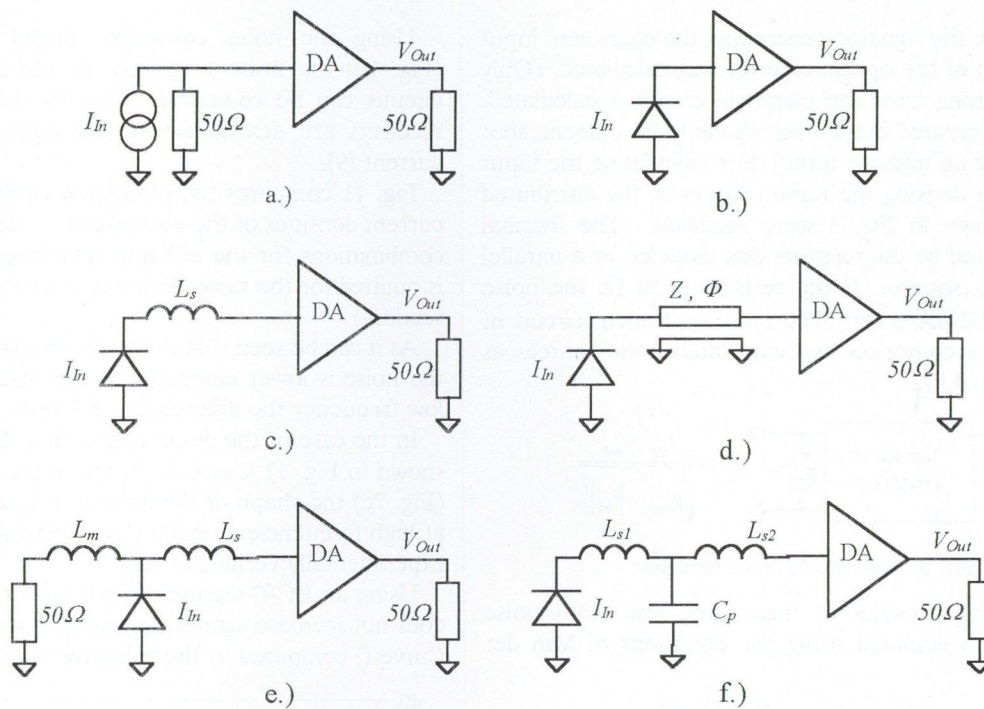

Fig. 7. Different matching circuits

Using a series inductance ($L_s = 625$ pH) to connect the diode to the amplifier (Fig. 7c), the gain can be more flat than in the direct connection, as it is shown in Fig. 8 Curve c.

The photodiode connected to the amplifier through a transmission line is drawn in Fig. 7d. If the electrical length (Φ) of the transmission line is small, the situation is similar to the inductive matching case (Fig. 7c). Supposing $Z \neq Z_0 = 50\Omega$ and Φ is great ($> \pi/2$), there are ripples in the gain at high frequencies. It is not depicted in Fig. 8 because the shape of the curve is depending either on Φ or on the transmission line impedance Z. The strong ripples in the response of the complete optical receiver can be avoided by using a short line.

Fig. 7e shows a T section matching with a resistive load ($L_m = L_s = 625$ pH). The gain has a peak (around 9 GHz) but it is 6 dB lower than the non-resistive matching.

Using an LC T-section ($L_{s1} = 1287$ pH, $L_{s2} = 312$ pH, $C_p = 0.35$ pF) for connecting the diode and the amplifier shown in Fig. 7f the gain can be more flat compared to the other non-resistive matching cases but has a 6 dB grater transfer impedance than the resistive matching.

From the above calculation, it can be seen that for high gain the best solution is a non-resistive matching when the PD is connected to the amplifier through an LC T-section (Fig. 7f).
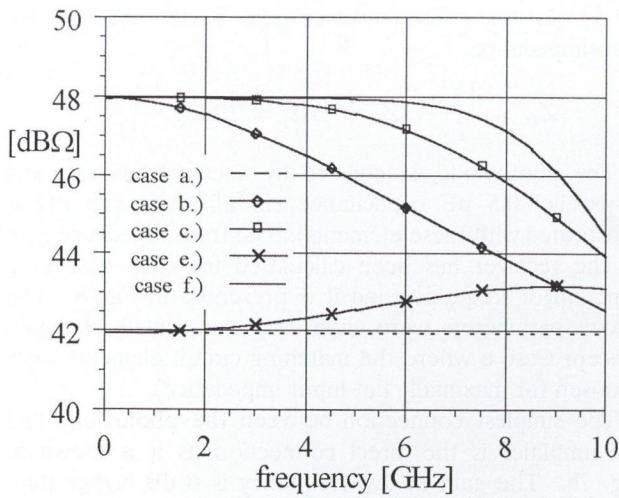
Fig. 8. Comparison of transimpedance gain

4. NOISE PROPERTIES

To describe the signal to noise ratio, the equivalent input noise current of the optical receiver was calculated. (Only the noise arising from the electrical circuit is calculated. The noise generated in the photodiode (dark current, shot noise) is only an additive term.) For calculating the input noise current density, the noise sources in the distributed amplifier shown in Fig. 3 were modeled. The thermal noise generated by the resistors was modeled by a parallel noise current source. If the resistor is 50 Ω, the noise current is 18.2 pA/$\sqrt{\text{Hz}}$. The noise equivalent circuit of the transistors comprises two correlated noise sources as shown in Fig. 9 [8].
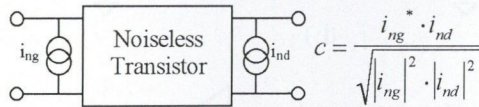

$$c = \frac{i_{ng}^{*} \cdot i_{nd}}{\sqrt{\left|i_{ng}\right|^2 \cdot \left|i_{nd}\right|^2}}$$

Fig. 9. Noise model of the transistor

The current densities of these gate and drain noise sources were calculated using the equations of Van der Ziel:

$$\overline{i_{ng}^2} = 4kT_0B\frac{\omega^2 C_g^2}{g_m}R$$

$$\overline{i_{nd}^2} = 4kT_0Bg_mP$$

where the parameters R and P are varying with drain current. It is shown that the correlation coefficient can be writen as: $c = c_r + i \cdot c_i = 0 + 0.35i$ [1]. Using the above equations the values of the noise currents have been calculated with $R = 0.2$, $P = 0.6$ and $c = 0.35i$.
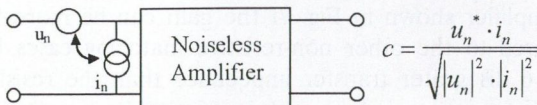

$$c = \frac{u_n^{*} \cdot i_n}{\sqrt{\left|u_n\right|^2 \cdot \left|i_n\right|^2}}$$

Fig. 10. Noise equivalent of the amplifier

Using latter noise models the noise of the four-stage distributed amplifier can be calculated. The noise of the

amplifier can be substituted with a correlated voltage and current noise source pair as shown in Fig. 10.

The calculated noise parameters of the amplifier as a function of the frequency are shown in Table 1.

Table 1. Calculated noise parameters of the DA

Freq. [GHz]	u_n [pV/$\sqrt{\text{Hz}}$]	i_n [pA/$\sqrt{\text{Hz}}$]	Correlation
1	257.067	18.669	0.226-0.369i
2	307.851	18.260	0.170-0.607i
3	374.163	17.595	0.115-0.732i
4	445.034	16.696	0.066-0.792i
5	513.896	15.600	0.020-0.817i
6	576.561	14.356	-0.024-0.816i
7	630.052	13.037	-0.072-0.794i
8	672.110	11.742	-0.127-0.744i
9	701.049	10.608	-0.189-0.657i
10	715.809	9.807	-0.256-0.526i

Using the noise equivalent model of the amplifier (Fig. 10) the noise properties of the different matching circuits can be compared. Usually the noise of optical receivers are described with the equivalent input noise current [9].

Fig. 11 compares the calculated equivalent input noise current densities of the photodiode − distributed amplifier combinations for the different matching circuits. (Case d is omitted for the same reason as described in the previous section.)

As it can be seen that in the non-resistive generator case the noise is lower compared to the resistive matching (at low frequency the difference is 3.3 dB).

In the case of the direct connection the noise current is shown in Fig. 11 Curve b. In the inductive matching case (Fig. 7c) the shape of the noise curve has a minimum but at high frequencies it has a steep increase. This result was experimentally verified as well.

Using an LC-T section the noise of the optical receiver does not increase significantly at high frequencies (Fig. 11 Curve f) compared to the inductive matching (Fig. 7c).
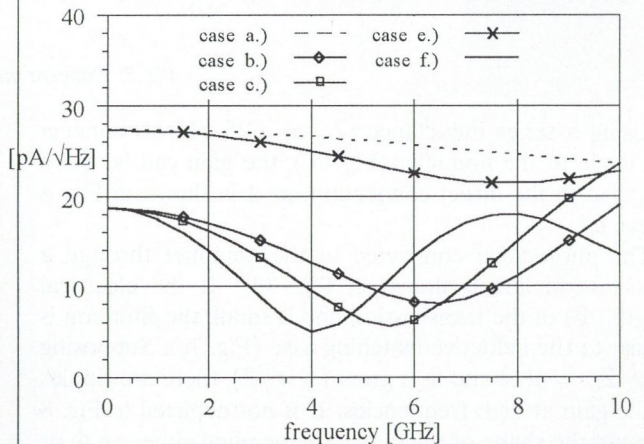

Fig. 11. Calculated equivalent input noise current densities

5. EXPERIMENTAL INVESTIGATION

The series inductive matching (see Fig. 7c) has been experimentally verified [10]. A hybrid integrated optical receiver was designed using distributed amplification. The receiver consists of a high speed photodiode and for simplicity only a two-stage distributed amplifier. The distributed amplifier was designed to provide 8 dB gain in a very broad band and a low noise figure.

The measurement set up consists of a HP network analyzer with a lightwave test set extension and a spectrum analyzer. The optical transmitter contains a DFB (distributed feedback) laser along with an external modulator. The optical wavelength is 1.3 μm and the modulation frequency is swept from 40 MHz to 12 GHz. That set up was used for characterizing the optical/microwave transfer performance of the optical receiver.

The measured responsivity of the optical receiver is relatively flat from 40 MHz up to 10 GHz. The measured equivalent noise current density of the optical receiver is depicted in Fig. 12 showing a low noise level. The shape of the curve follows the theoretical one.

6. CONCLUSION

Various matching circuits connecting a photodiode to a distributed amplifier have been analyzed and compared. As a conclusion the optical receiver applying resistive matching has 6 dB less amplification and greater noise

than the others. Comparing the five analyzed circuits, the best solution is the non-resistive LC T-section (Fig. 7f) considering both the gain and noise performance.
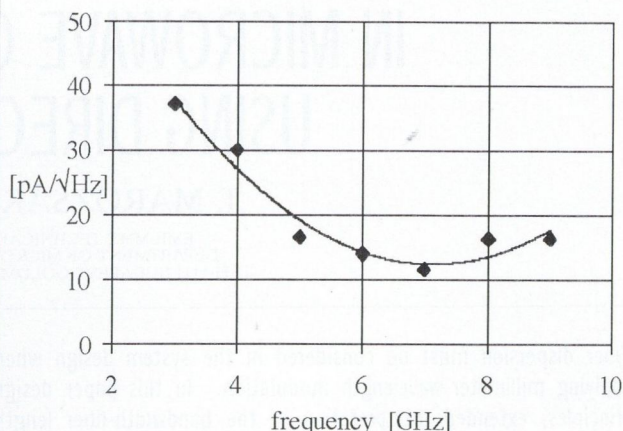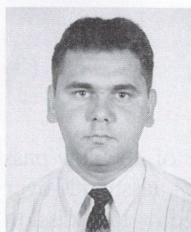

Fig. 12. Measured equivalent input noise current density of the optical receiver

7. ACKNOWLEDGMENT

REFERENCES

[1] C. S. Aitchison: "The Intrinsic Noise Figure of the MESFET Distributed Amplifier", *IEEE Transactions on Microwave Theory and Techniques*, Vol. 33, No. 6, pp. 460-466, June 1985.

[2] A. Zólomy, A. Hilt, A. Baranyi, G. Járó: "Microwave Distributed Amplifier in Hybrid Integrated Technology", *Proc. of the ECCTD'97*, Hungary, Sept. 1997.

[3] G. Járó, A. Zólomy, T. Berceli, J. Ladvánszky, A. Baranyi, C. S. Aitchison and J. Y. Liang: "Noise Minimization in Photodiode Driven Distributed Amplifiers", *Proc. of the 25th European Microwave Conference*, pp. 179-184, Bologna, Italy, Sept. 1995.

[4] K. Yang, A. L. G.-Aitken et al.: "Design, Modelling, and Characterization of Monolithically Integrated InP-Based (1.55 μm) High-Speed (24 Gb/s) p-i-n/HBT Front-End Photoreceivers", *IEEE J. of Lightwave Techn.*, Vol. 14, No. 8, pp. 1831-1839, Aug. 1996.

[5] A. Hilt, G. Járó, A. Zólomy, B. Cabon, T. Berceli and T. Marozsák: "Microwave Characterization of High Speed pin Photodiodes", *Proc. of the COMITE'97*, Czech Republic, October 1997.

[6] T. Y. Wong: "Fundamentals of Distributed Amplification", *Artech House*, Boston, London, 1993.

[7] Helsinki University of Technology: "APLAC: Analysis Program for Linear Active Circuits", version 6.2, Espoo, Finland.

[8] A. Ambrózy: "Electronic Noise", Akadémiai Könyvkiadó, Hungary, 1982.

[9] A. K. Petersen, F. Ebskamp, R. J. S. Pedersen, X. Zhang: "Wide-band Low-Noise Distributed Front-End for Multi-Gigabit CPFSK Receivers", *IEEE MTT-S Digest*, pp. 1375-1378, 1994.

[10] A. Zólomy, T. Berceli, A. Hilt, G. Járó, C. Aitchison, A. Baranyi, J. Ladvánszky and J. Y. Liang: "Eight-Octave Bandwidth Optical Receiver Using Distributed Amplification", *Proc. of the IEEE MTT-S Topical Meeting on Optical Microwave Interactions*, Duisburg, Germany, Sept. 1997.

Gábor Járó received the M. Sc. degree in electrical engineering from the Technical University of Budapest in 1994. In 1994 he joined the Department of the Microwave Telecommunication, TUB, where he is working toward his Ph.D. degree. His research interest are in the areas of noise in high speed optical receiver and optical system, millimeter-wave signal generation in optical systems.
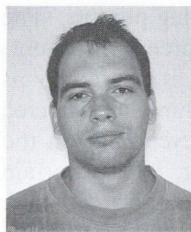
Attila Hilt for a photograph and biography, see p. 30.

Attila Zólomy received the M. Sc. degree in electrical engineering from the Technical University of Budapest in 1994. Now he is working at the Department of Microwave Telecommunication as a Ph.D. student. His research interest are in the field of wideband microwave distributed amplifiers, high speed photodetectors, millimeter-wave signal generation in optical systems.

Tibor Berceli for a photograph and biography, see p. 1.

SINGLE MODE FIBER DISPERSION
IN MICROWAVE OPTICAL SYSTEMS
USING DIRECT DETECTION

T. MAROZSÁK and S. MIHÁLY

BME-MHT, TECHNICAL UNIVERSITY OF BUDAPEST
DEPARTMENT OF MICROWAVE TELECOMMUNICATIONS
H-1111 BUDAPEST, GOLDMANN GYÖRGY TÉR 3., HUNGARY

Fiber dispersion must be considered in the system design when applying millimeter-wavelength modulation. In this paper design principles, extended interpretation of the bandwidth-fiber length product and a simple novel type dispersion measurement method using microwaves are presented.

1. INTRODUCTION

There is a growing demand in transmitting millimeter-waves over optical fibers. The subcarrier multiplexed systems and optical-radio systems can operate at frequencies above 10 GHz. For these applications electro-absorption modulators offer a bandwidth of tens of gigahertz [1]. Passively mode-locked monolithic semiconductor lasers can provide pulses at repetition rates well beyond the modulation bandwidth of semiconductor lasers [2].

The optical fiber as a system element usually supposed to behave like a Gaussian low-pass filter. This give a limit in the usable frequency bands, which is already widely investigated [3]−[5]. Here the possibility of using the existing, cheap, not dispersion compensated fiber systems with direct detection in microwave systems is discussed. Utilizing a scalar measurement apparatus, a novel type of dispersion measurement is also presented.

2. THEORY

The pure silica fiber has no first order dispersion around 1300 nm and it has less then $20 \; \frac{\text{ps}}{\text{km}\cdot\text{nm}}$ at 1550 nm. Even this small value must be taken into account in microwave systems, were millimeter-wave modulation signals have to be detected. The intensity modulation of the light having Ω frequency with a microwave modulating signal of ω frequency causes, that two sidebands appear at $\Omega + \omega$ and $\Omega - \omega$. This means three separate optical signal differing in wavelength, if narrow linewidth laser is assumed. This difference can be so large, that the dispersion of the fiber makes sufficiently long delay between them. The time delay means phase shift of the representing phasors. The total electric filed is the sum of the three components in the receiver and the detected signal is related to its envelope because of direct detection. Thus, the detected power depends on the phase shifts and eventually on the lengths and the dispersion of the fiber. In a certain situation the ω frequency signal can not be detected. Fig. 1 shows the calculated transfer characteristic which is defined as

$$G(\omega) = \frac{I_{\text{detected}}(\omega)}{I_{\text{modulation}}(\omega)} \qquad (1)$$

where I means current and the optical to electrical conversion assumed to be ideal. In Fig. 1 100 km long fiber is calculated with $3 \frac{\text{ps}}{\text{km}\cdot\text{nm}}$ dispersion using 1550 nm source. In the calculations the attenuation of the fiber was neglected and the linewidth enhancement factor was assumed to be zero because of using external modulation.

This optical fiber model is not linear. At frequencies where the transfer function starts to decrease, higher order harmonics appear which must be taken into account in the system design.
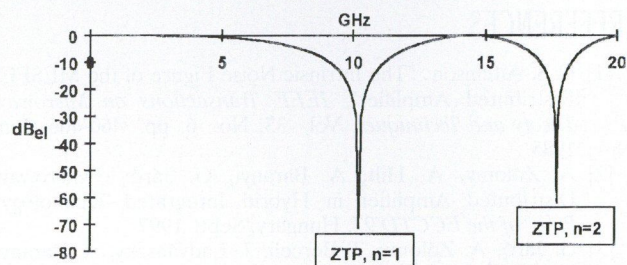

Fig. 1. Calculated transfer characteristic of a fiber at millimeter wavelengths

Design principles can be derived with this mathematical model for microwave-optical systems. In case of baseband applications the 3 dB bandwidth of the fiber is:

$$B = \frac{\nu}{\sqrt{(8DLc + 1)}} \qquad (2)$$

where D is the total chromatic dispersion of the single mode fiber, c is the speed of light in vacuum, L is the length of the fiber and ν is optical frequency. The bandwidth-fiber length product can be approximated from (2) with:

$$L \cdot B^2 = \frac{c}{8D\lambda^2}, \qquad (3)$$

λ is optical wavelength.

If this fiber approach is used instead of the low-pass Gaussian filter approach, there are several passbands over the baseband. These are situated after zero transmission points (ZTP), which are getting closer as the frequency increases. The frequency of the zero transmission points

(ZTP) of the optical media can be calculated to exclude that ranges from the modulation band:

$$f = \sqrt{\frac{k}{4DLc - k}} \cdot \nu \qquad (4)$$

where k is an even integer and corresponds to the n_{th} ZTP as $k = 2n - 1$. Using the k number, the bandwith-fiber length product can get a new interpretation. The start frequency and the bandwidth of the passband between the n and $(n+1)$ th ZTP is:

$$f = \sqrt{\frac{k}{8DLc - k}} \cdot \nu \ ,$$

$$B \cong \frac{\sqrt{k+2} - \sqrt{k}}{\sqrt{8DLc - k}} \cdot \nu \ , \ k = 4n - 1 \ . \qquad (5)$$

Increasing the fiber length or the dispersion, the bandwidth of these passbands decreases similarly to the baseband. The bandwidth − length product corresponding to the passband above the n_{th} ZTP:

$$L \cdot B^2 \cong \frac{k + 1 - \sqrt{k^2 + 2k}}{4Dc} \cdot \nu^2 \ . \qquad (6)$$

This value is always less than in the baseband, but the fiber capacity can be increased over its usual baseband limit by using these frequency ranges.

This theory can be used for simple dispersion measurements also. Solving the transfer function for D gives:

$$D = \frac{k(\nu^2 - f^2)}{4(Lcf^2)} \qquad (7)$$

where f is ZTP. $k = 2n - 1$ refers here to the higher order ZTPs, which are spaced closer to each other as f increases. When there are more of them in the measured frequency range, the random errors can be reduced with taking all into account.

3. MEASUREMENTS

The measurement set-up can be seen in Fig. 2. The advantage of this set-up is the usage of simple scalar detection.
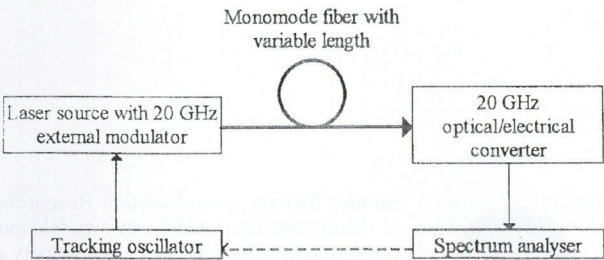

Fig. 2. Measurement setup

Measurements were taken with different lengths of fibers. The light of a 1550 nm, 40 MHz linewidth DFB laser source was intensity modulated by an external modulator having 20 GHz bandwidth. After the high speed

optical receiver a spectrum analyzer with tracking oscillator was used providing large dynamic range. In Fig. 3 the measured and the calculated transmission characteristics can be seen. The results show very good agreement with the theory.

Fig. 4 shows a measurement result with two ZTP. The calculated total chromatic dispersions, calculating from (7), are $D = 8.775 \frac{\text{ps}}{\text{km} \cdot \text{nm}}$ and $D = 8.7 \frac{\text{ps}}{\text{km} \cdot \text{nm}}$ for $k = 1$ and $k = 3$, respectively, which are in good agreement.
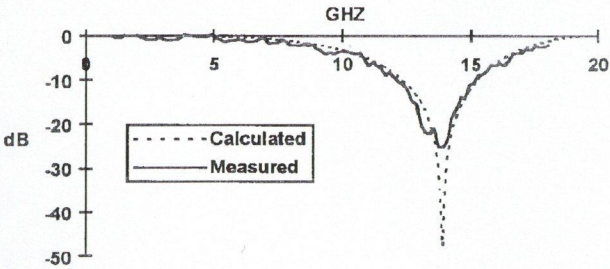

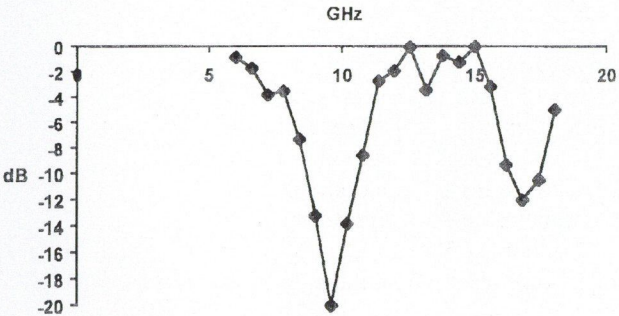Fig. 3. Measured and caldulated fiber transmission, $L = 18$ km, $D = 9 \frac{ps}{(km \cdot nm)}$

Fig. 4. Measured transmission, $L = 38.6$ km

4. CONCLUSIONS

The simple, not dispersion compensated fiber can be used in microwave systems if dispersion is taking into account. Simple design principles were derived for the dispersive fiber. Experimental results show the validity of this simple fiber model. Utilizing it dispersion measurements can be easily performed with commercially available equipment by making scalar measurements.

5. ACKNOWLEDGMENT

REFERENCES

[1] Tatemi Ido: "Ultra High Speed Multiple-Quantum-Well Electro-Absorption Optical Modulators with Integrated Waveguides", *Journal of Lightwave Technology*, Vol. 14, No. 9, September 1996.

[2] T. Hoshida: "Extremely Low-Amplitude Modulation in a Sub-harmonically Hybrid Mode-Locked Monolithic Semiconductor Laser", *IEEE Photonics Technology Letters*, Vol. 8, No. 9, September 1996.

[3] John M. Senior: *Optical Fiber Communications — Principles and Practice*, Prentice Hall, 1992, second edition.

[4] A. F. Elrefaie: "Chromatic Dispersion Limitations in Coherent Lightwave Transmission Systems", *Journal of Lightwave Technology*, Vol. 6, No. 5, May 1988.

[5] Jiang Song: "A Simplified Dispersion Limit Formula for IM/DD Systems and its Comparison with Experimental Results", *Journal of Lightwave Technology*, Vol. 13, No. 3, March 1995.
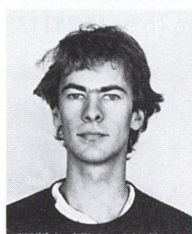
Tamás Marozsák graduated at the Faculty of Electronic Engineering and Informatics of the Technical University of Budapest in 1995. His recent research related to the field of optical communications. From 1995 he is PhD student at the Department of Microwave Telecommunications of the Technical University of Budapest.
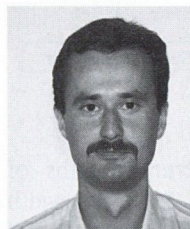
Sándor Mihály is an Assistant Researcher at the Department of Microwave Telecommunications of the Technical University of Budapest. He graduated from the TUB in 1984 and was a postgraduate student of the Hungarian Academy of Sciences between 1984–1987. He became a member of the Department of Microwave Telecommunications in 1987, from then on he has been participating in the educational and research activities of the department. His main fields of research are agricultural and earth observation applications of active microwave airborne and spaceborne remote sensing, combined optical and microwave communication systems, subsystems and circuits. He is Member of IEEE and the Scientific Society for Telecommunication.

A CONTINUOUS-TIME LOGARITHMIC PHOTORECEPTOR CELL FOR PARALLEL VLSI IMAGE PROCESSING

M. OLÁH and L. LIPTÁK-FEGÓ

DEPARTMENT OF ELECTRON DEVICES
TECHNICAL UNIVERSITY OF BUDAPEST
H-1521 BUDAPEST, HUNGARY

A continuous-time current-output programmable-gain logarithmic photoreceptor cell that we have designed for a standard digital CMOS IC process is presented. The cell can be integrated with on-chip pro- ceasing units, thus can be used as a front-end to a highly parallel continuous-time processing array. Functional parts of the circuit have been fabricated and tested. The design of the photoreceptor cell and a method we have developed to spatially scan the electrical response of photosensitive circuits versus optical stimulus are described. Measured characteristics of transconductance amplifier of the cell have been verified with simulation results.

1. INTRODUCTION

Recent opportunities in information technology open markets for small-size, battery operated portable systems. A desired feature of such systems is the direct (sensory) interface to the people and/or the highly variable environment which requires high computational throughput due to variability and noise, while still maintaining it at low power due to portability [1]. The computational and power efficiency of natural biological systems suggests that our artificial sensory information processing systems should be based on functional and architectural principles of their biological counterparts. Low-precision analog VLSI (very large scale integration) seems to be the ideal medium to implement neuromorphic systems if power-consumption, area, and cost are of some concern [2]. Integrated signal processing systems, with on-chip photosensing devices based on the above design concepts have been built (e.g. early vision processing [3], video data compression [4]). These systems solve task which otherwise expensive with the conventional CCD image-grabber, digital signal processing arrangement.

We have designed a continuous-time, logarithmic photoreceptor cell in CMOS integrated circuit technology. The circuit implements biologically motivated functions using conservative devices and circuit techniques. Gain-programmability, threshold adjustment makes it suitable to integrate with processing elements and form a highly-parallel continuous-time processing array, such as CNN [5].

2. ARCHITECTURE AND CIRCUIT DESIGN

The biological light sensors share some characteristic features, which should be implemented in our receptor, too [6]. These are: (*i*) logarithmic response to illumination, (*ii*) adaptivity to different lighting conditions, (*iii*) higher sensitivity to rapidly varying signals. The architecture of our receptor can be seen on Fig. 1.
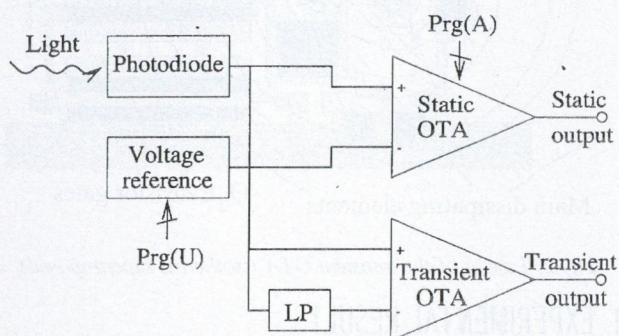

Fig. 1. Block diagram of the sensor

The photosensitive device is a simple pn-junction operating in photo-voltaic mode: its open-loop voltage is proportional to the *logarithm* of the intensity of the incident light. The signal of the sensor is amplified by two separate stages. The static OTA (Operational Transconductance Amplifier) produces an output current proportional to the difference between the voltage of the photodiode and an programmable reference. The gain of the static OTA can be set digitally from 0 to 3 times of its nominal transconductance with a resolution of 0.5. The *transient OTA* amplifies the *rapid changes* of the photo-signal by taking its low-pass filtered version as the reference (i.e. *adapting* to the signal dc level).

3. LAYOUT DESIGN

The chosen fabrication technology is a low-cost, digital CMOS process. The parts were layed out in unit-size blocks ('standard cell's) adding the flexibility of building different structures.

Each pn-junction of the circuit is sensitive to light, therefore not only the desired photodiode responds. To minimize the side-effects, the entire surface except the photodiode was covered with the second metal layer being an efficient shield against the light.

The transconductance amplifier is subject to temperature changes. Since its input offset voltage mainly arises from the mismatch (both thermal and geometric) of the input transistor pair their shape and topology with respect to the main dissipating elements is crucial. Therefore the gates of the input pair in the transient OTA are arranged

match along them. The THERMANAL thermal simulation tool proved, that the corresponding points of the transistor gates are on isotherms (Fig. 2) For the appropriate operation of OTAs, which means symmetric characteristics, the random offset of current mirrors is to be minimized. Therefore each pair of transistors should be close to each other and have to be identical both in size and shape. All these constraints were used during the layout design.
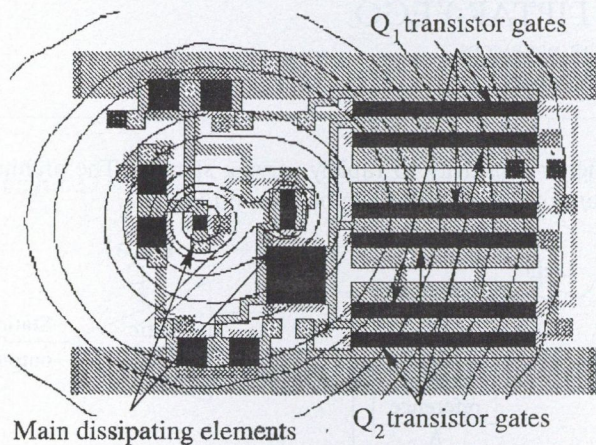

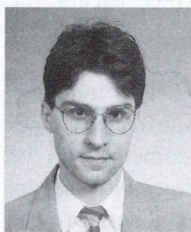*Fig. 2. Layout of the transient OTA (isotherms superimposed)*

4. EXPERIMENTAL RESULTS

Four different size n-well/bulk photodiodes and the transient OTA with the LP filter have been fabricated in 1.0 μm ES2 process.

Diffusion of photogenerated minority carriers can affect low-current circuits (e.g. LP filter). Therefore we placed the chip on a motorized x-y table and imaged a light spot onto the silicon surface through a pinhole with a $50\times$ lens microscope to spatially scan the electrical response of sensitive parts versus photo-stimulus. The diameter of the spot was calibrated with known sizes of layout features (6 μm). Positioning and synchronized data acquisition was controlled by a PC.

REFERENCES

[1] A. G. Andreou: Low power analog VLSI systems for sensory information processing. In M. Ismail B. Sheu, Edgar Sanchez-Sinencio, editor, *Microsystems Technologies for Multimedia Applications: An Introduction*. IEEE Press, Los Alamitos CA, 1995.

[2] E. A. Vittoz: Analog VLSI signal processing: why, where, and how? *Journal of VLSI signal processing*, (8):27-44, 8 1994.

[3] C. Mead: *Analog VLSI and Neural Systems*, Addison-Wesley, Reading, MA, 1989.

First, we measured the short circuit current of the test photodiodes with a Keithley 616 electrometer as we moved the light spot around. The SEM image of the four diodes and the optical scan of one diode can be seen on Fig. 3. The pn junction sinks the photogenerated excess of minority carriers thus can be used as a probe for measuring their local concentration. Minority carrier concentration in the bulk around the light spot was measured by moving the spot away from the probe. A simple decaying exponential was fitted on the data giving a 70 μm space constant (empirical diffusion length). Second, the effect of light measured as the input offset of the amplifier was found insignificant. Measured DC parameters ($g_m = 136$ μmho, $I_{sat} = 27$ μA, $g_{out} = 0.4$ μmho) were in good agreement with the simulation results. However we ran into problems with measuring the transient behaviour of the amplifier with the LP filter. Probably the current load of pad circuitry used to access on-chip components can be accounted for this. This should be taken into account in further designs.
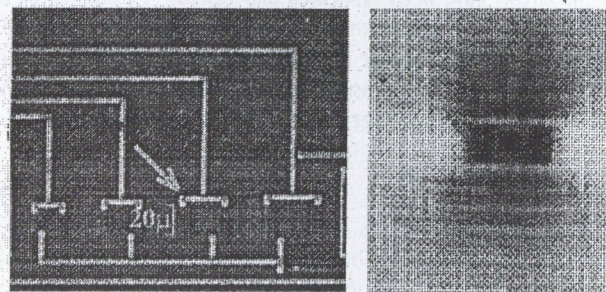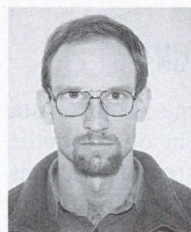

Fig. 3. Scanning Electron Microscope (left) and optical scanned (right) image of test photodiode(s). Darker pixel refers to higher photocurrent on right image.

5. ACKNOWLEDGMENT

[4] T. Hamamoto, M. Hatori, K. Aizawa, H. Ohno and J. Yamazaki: A novel image sensor for video compression, *Proceedings ICIP*, 3:591-595, 1994.

[5] L. O. Chua and T. Roska: The CNN paradigm, *IEEE Trans. on Circuits and Systems-I*, 40(3):148-156, March 1993.

[6] T. Delbrück: *Investigations of Visual Transduction and Motion Processing*. PhD thesis, Computation and Neural Systems Program, Caltech, 1993.

Miklós Oláh (M.Sc.Eng.) has received the M.Sc. degree in electrical engineering at the Technical University of Budapest, Hungary in 1994. Currently he is working at the Hungarian Academy of Sciences, Institute of Isotopes, Dept. of Chemical Physics, and is a Ph.D. student of the Technical University of Budapest, Department of Electron Devices. His field of interest concerns mixed-signal VLSI implementation of parallel systems for image processing and control.

László Lipták-Fegó is a graduating electrical engineering student at the Technical University of Budapest. His major is microelectronics and covers design and simulation of analog and VLSI integrated circuits. Some of his chips have already been fabricated and tested successfully.

TKI·))))

TELECOMMUNICATION INNOVATION COMPANY LTD

Civil and defence purpose equipment:
- development, manufacture, engineering services

Electronic surveillance:
- microwave telecom equipment
- microwave panorama receiver and analyser
- demultiplexers: frequency division, time division up to 45 Mbit/s
- compression type receivers, radar surveillance

Communication security:
- fax, phone and data signals
- encryption of multichannel data up to 2 Mbit/s speed

Special microwave materials and components:
- microwave circulators, isolators
- ferrite materials

Complex engineering services for telecommunication network installations

Designing, installation:
- network designing, designing microwave links
- selecting sites – preparing plans for permits
- developing operating and maintenance plans
- developing installation plans – logistical planning
- clearance, storing, bank guarantees, insurance
- on site material handling and inventory management

Co-operation with suppliers:
- site surveys – installing indoor and outdoor equipment
- commissioning, tuning – testing links
- system testing – test laboratory

Program management

Training

Guarantee and maintenance tasks

Ensuring inspection system

Laboratory measurements:
- manufacturer checking, measurements of links

Organising and executing civil engineering works

References:
- Antenna Hungaria, MOL, Postabank, Westel 450, Pannon GSM, MATÁV, Motorola RLL

Under preparation:
- installing European mobile networks, installing, operating EKHZ and its security

Address:

TKI Telecommunication Innovation Co. Ltd
H-1142 Budapest, Ungvár u. 64-66.
Phone: (361)-251-0888; Fax: (361)-251-9878; E-mail: tki@tki.hu

SIEMENS

Budapest, 1997. szeptember 12.

Kedves Olvasó!

A Siemens, a világ egyik legnagyobb elektrotechnikai vállalata, amely már 110 éve jelen van Magyarországon is, ezekben a hetekben ünnepli megalapításának 150. évfordulóját. 198 országban 400.000 munkatársának napi partnere több milliárd ember. Hihetetlen? Vegyük csak a magyar példát. Tudja-e Ön például azt, hogy

- a *millenniumi földalattit* és a *körúti 6-os előbjét* is a Siemens építette?
- Budapest több mint 300 *közlekedési csomópontját* Siemens berendezés irányítja?
- a *Lágymányosi híd különleges megvilágítása* is Siemens konstrukció?
- jelenleg a MÁV Rt. 300 km-es szakaszának *villamosításán* dolgozunk?
- a MÁV Rt. *távközlési hálózatát* optikai szálakkal a Siemens Telefongyár korszerűsíti?
- a Paksi Atomerőmű *reaktorvédelmi berendezéseit* a Siemens újítja fel?
- elektromos energiahálózatunk *üzemirányítása* Siemens rendszerben történik?
- sok magyar vállalat *termelési folyamatait* is Siemens rendszerek irányítják?
- háromszor is elérné a Holdat a Magyar Kábel Művek gyártotta évi *kábel és vezeték*?
- Szombathelyen, Cegléden, Bicskén high tech színvonalú *komponensgyártás* folyik?
- már több mint egymillió előfizető Siemens *telefonközpontokhoz* van bekötve?
- több mint 3.000 Siemens *telefonalközpont* több mint 100.000 mellékállomást szolgál ki?
- több mint 200.000 Siemens *telefonkészüléket* használnak honfitársaink?
- *computer tomográfok, szívkatéter* állomások között a legtöbb Siemens termék?
- a magyar lakások százezreiben működik valamilyen Siemens *háztartási gép*?
- Siemens Nixdorf *számítógépek* segítik a népesség- és a gépjármű-nyilvántartást is?
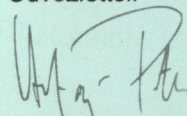
A Siemens a világ első számú *fővállalkozó-rendszerintegrátora*: a részterületek csúcs-technológiája - az együttműködés, a tapasztalat, a munkamódszer mellett - elenged-hetetlen feltétele a *rendszerek egésze magas színvonalának*. Ehhez évi 7 milliárd márkát, azaz napi *3 milliárd forintot* költ *kutatás-fejlesztésre*, amivel *45.000 munkatárs* foglalkozik.

A legtöbb országban úgy mondják: Siemens - always a bit more.
Mi itthon így mondjuk: **Siemens - többet tudunk, többet nyújtunk.**

A 23 magyarországi Siemens vállalat több, mint négyezer munkatársa nevében ezúton is köszöntöm valamennyi partnerünket, köszönöm megbízásukat, bizalmukat.
Azért dolgozunk, hogy a jövőben is elégedettek legyenek velünk.

Üdvözlettel:

Hetényi Péter
Siemens csoport
Magyarország